

A consistency test of spectroscopic gravities for late-type stars

Carlos Allende Prieto¹ and Ramón J. García López

Instituto de Astrofísica de Canarias

E-38200, La Laguna, Tenerife,

SPAIN

David L. Lambert

McDonald Observatory and Department of Astronomy,

The University of Texas at Austin

RLM 15.308, Austin, TX 78712-1083,

USA

Bengt Gustafsson

Uppsala Astronomical Observatory

Box 515, S-751 20 Uppsala

SWEDEN

Received _____; accepted _____

¹Present address: McDonald Observatory and Department of Astronomy, The University of Texas at Austin, RLM 15.308, Austin, TX 78712-1083, USA

ABSTRACT

Chemical analyses of late-type stars are usually carried out following the classical recipe: LTE line formation and homogeneous, plane-parallel, flux-constant, and LTE model atmospheres. We review different results in the literature that have suggested significant inconsistencies in the spectroscopic analyses, pointing out the difficulties in deriving independent estimates of the stellar fundamental parameters and hence, detecting systematic errors.

The trigonometric parallaxes measured by the *Hipparcos* mission provide accurate appraisals of the stellar surface gravity for nearby stars, which are used here to check the gravities obtained from the photospheric iron ionization balance. We find an approximate agreement for stars in the metallicity range $-1.0 \leq [\text{Fe}/\text{H}] \leq 0.$, but the comparison shows that the differences between the spectroscopic and trigonometric gravities decrease towards lower metallicities for more metal-deficient dwarfs ($-2.5 \leq [\text{Fe}/\text{H}] \leq -1.0$), which casts a shadow upon the abundance analyses for extreme metal-poor stars that make use of the ionization equilibrium to constrain the gravity. The comparison with the strong-line gravities derived by Edvardsson (1988) and Fuhrmann (1998a) confirms that this method provide systematically larger gravities than the ionization balance. The strong-line gravities get closer to the physical ones for the stars analyzed by Fuhrmann, but they are even further away than the iron ionization gravities for the stars of lower gravities in Edvardsson's sample.

The confrontation of the deviations of the iron ionization gravities in metal-poor stars reported here with departures from the excitation balance found in the literature, show that they are likely to be induced by the same physical mechanism.

Subject headings: radiative transfer – techniques: spectroscopic – stars: atmospheres – stars: distances – stars: fundamental parameters – stars: late-type

1. Introduction

Interpretation of stellar spectra to quantify chemical abundances requires, among other ingredients, the use of model atmospheres, and our knowledge of the physics they are built on will determine the accuracy of the analyses. Following the standard method, measurements of equivalent widths or line profiles at high resolution and high signal-to-noise ratio are analyzed using a classical model atmosphere based on the following assumptions: local thermodynamic equilibrium (LTE), hydrostatic equilibrium, conservation of flux, and plane-parallel stratification. Also, the mixing-length theory is used to take convection into account. Finally, a chemical composition is assumed, and the non-thermal broadening of spectral lines is treated by a simplified recipe: micro and macro turbulence (for a review see, e.g. Gustafsson & Jørgensen 1994).

Such standard analyses may be subjected to external and internal consistency checks. Often, such a check involves a determination of a stellar parameter by two or more methods. An inconsistency may indicate either an inadequate implementation of the methods for deriving the stellar parameters or a failure of one or more of the assumptions on which the models are built. Of course, both contributors of inconsistencies may operate simultaneously, and in some cases, the distinction between them may be subtle. If the implementation of the separate methods is accurate, consistent results for a stellar parameter is a necessary but not a sufficient indication that a given model atmosphere is a reliable representation of the real atmosphere.

Important failures to reproduce observations have been claimed, even for the Sun and other solar-like stars. The $H\alpha$ and $H\beta$ wings of the solar spectrum cannot be reproduced by some theoretical models using a typical value for the mixing-length parameter $\alpha \sim 1.5$, as noticed by Fuhrmann, Axer & Gehren (1993) and Van't Veer-Menneret & Megessier (1996). They suggest a lower value for α , but this has been rejected by Castelli, Gratton

& Kurucz (1997), who showed that the predicted flux distribution is not in agreement with observations. This failure might just be classified as an inadequate implementation of the classical method.

Tests on the consistency of surface gravities derived by different procedures have been reported in the literature. Brief remarks on three such tests must suffice here. Edvardsson (1988) discovered from the analysis of a sample of eight sub-giants that the ionization equilibrium of iron and silicon, as derived from weak neutral and ionized lines, gave gravities systematically lower than those obtained from the pressure-broadened wings of strong metal lines. Even more striking was the discrepancy presented by Fuhrmann et al. (1997; also Steffen 1985) for Procyon. They found $\log g = 3.5$ (in c.g.s. units) from the ionization equilibrium of iron, in strong contrast to the much higher values they derived from the wings of strong lines and the astrometric measurements: $\log g \simeq 4.05$. Gratton, Carreta & Castelli (1996) derived gravities for giants in globular clusters using theoretical isochrones, and compared them with the spectroscopic gravities (requiring ionization equilibrium), detecting large differences for lower effective temperatures. The results of Nissen, Høg & Schuster (1997) suggest that the spectroscopically derived gravities in the literature are systematically lower than those derived from *Hipparcos* (ESA 1997) parallaxes for the metal-poor stars in the gravity range $3.5 \leq \log g \leq 4.5$.

Very recently, Fuhrmann (1998a) has carried out a similar check of the spectroscopically derived gravities, using them to estimate *spectroscopic* distances which he compares with the *Hipparcos* data for nearby (i.e. with highly accurate parallaxes) stars. This kind of comparison is equivalent to that of Nissen et al. (1997) but using distances instead of gravities. His analysis covered stars in the metallicity range² $-1.95 \leq [\text{Fe}/\text{H}] \leq +0.40$ and

² $[\text{M}/\text{H}] = \log\left(\frac{N(\text{M})}{N(\text{H})}\right) - \log\left(\frac{N(\text{M})}{N(\text{H})}\right)_{\odot}$ where $N(\text{M})$ is the number density of the nuclei of the element M and "H" refers to hydrogen.

gravities running the gamut from $\log g = 3.1$ to 4.7. He finds an impressive agreement between distance estimates, as indicated by the mean difference which is a mere 3.4 %, with a scatter of 4.9 % (after rejecting a few outliers). This result is not in contradiction with the differences found by Nissen et al. (1997), as the spectroscopic gravities of Fuhrmann were not derived from the ionization equilibrium only, but a combination of this estimator with the pressure sensitive wings of strong singly ionized metal lines. The discrepancy between the two methods was confirmed again for the hotter stars, for which the strong-line gravities were preferred.

Another series of consistency checks involves the stellar effective temperatures (T_{eff}). Observationally, the checks exploit either the flux distribution or the excitation of a species (Fe I, for example) well represented by weak lines in the stellar spectrum. Again, a few examples must suffice here. Magain (1985) found discrepancies between the ultraviolet fluxes predicted by the models and the observations for two metal-poor stars (see also Gustafsson & Bell 1979), although Bell & Oke (1986) arrived at the opposite conclusion. Magain & Zhao (1996) reported strong correlations between iron abundances and the excitation potential of the employed spectral lines of neutral iron, i.e., the Fe I excitation temperature is not that predicted by the classical model of the photometry-based (b-y and V-K calibrations from Magain 1987) effective temperature. They quantified the departures from the excitation equilibrium and mapped them on the $T_{\text{eff}} - \log g$ plane, finding smooth variations of the slope of the derived iron abundance against the excitation potential. However, we note that the metal-poor sub-giant HD140283, as analyzed by Magain (1984), exhibits a slope of the iron abundance with excitation potential in the opposite sense to that expected from the position of the star in the $T_{\text{eff}} - \log g$ diagram and the picture drawn by Magain & Zhao (1996). Analysis of the excitation balance in the metal-poor giant HD122563 by Dalle Ore (1993) showed that departures were present, and Gratton et al. (1996) found that the departures do not depend on gravity.

However, conclusions must be extracted with extreme care. The situation is especially complex, as many factors influence the consistency tests. Errors in the photometric effective temperatures, inadequacies in the damping treatment, or systematic errors in the atomic data or the spectroscopic measurements are enough to produce an apparent disagreement, which might be wrongly interpreted as a fault of the model atmospheres.

Devotees of metal-poor stars wonder if the suggested inconsistencies, often demonstrated for more metal-rich stars too, are more or less severe for their favorite stars that hold the keys to the chemical evolution of the early Galaxy. As pointed out by Gustafsson & Jørgensen (1994), or Magain & Zhao (1996), two points seem to be especially critical for the low metallicity stars:

a) LTE: due to the low metallicity and the therefore much weaker metal-absorption in the ultraviolet, a more non-local UV flux is able to penetrate from the deeper layers. This flux is vital in determining the ionization equilibrium of the atoms. As a consequence, the role of radiation on the thermodynamical state of matter becomes more important, resulting in stronger deviations from LTE.

b) Inhomogeneities: the lower H^- due to diminished amount of electrons makes the atmosphere more transparent so that the effects of convection can be more clearly seen in the photosphere. This is suggested by the results of Allende Prieto et al. (1995, 1999), who found convective line asymmetries to be stronger than expected in the metal-poor subgiant HD140283.

These two points could be even more critical for the low-gravity stars where, due to the low densities, both deviations from LTE and convective temperature inhomogeneities may be enhanced.

In this work, we have extended the analysis of trigonometric gravities to many stars

for which spectroscopic gravities had been previously estimated from the iron ionization equilibrium. Assessment of the spectroscopic gravity scale should be considered a mandatory step, to properly connect chemical abundances of stars in globular clusters, which are derived from the spectra of red giants, with those of fields halo stars, which come from dwarfs or slightly evolved subgiants.

2. ‘Trigonometric’ Gravities

The newly available *Hipparcos* parallaxes have provided distances to many stars in the solar neighborhood. These measurements allow us to constrain the stellar gravities. In this section, the trigonometric gravities are compared with the gravities obtained spectroscopically from the neutral and ionized iron lines. Our goal is to verify the results of Nissen et al. (1997), extending their study to many more stars, and to determine if the differences between trigonometric and spectroscopic gravities depend primarily on gravity, metal content, temperature, or a combination of all three parameters.

The scheme uses the familiar relationships: $g \propto M/R^2$ and $L \propto R^2 T_{\text{eff}}^4$, where M , R , and L are the stellar mass, radius, and luminosity, respectively. Straightforward manipulation gives

$$\log \frac{g}{g_{\odot}} = \log \frac{M}{M_{\odot}} + 4 \log \frac{T_{\text{eff}}}{T_{\text{eff},\odot}} + 0.4V_0 + 0.4BC + 2 \log \pi + 0.12, \quad (1)$$

where the π is the parallax, V_0 the apparent Johnson V magnitude, and BC the bolometric correction. Nissen et al. (1997) have already applied *Hipparcos* parallaxes in this way – see also Fuhrmann (1998b) – and we have followed their recipe. Alternatively, Equation 1 may be used to derive a spectroscopic parallax from a spectroscopic gravity, as done by Fuhrmann (1998a). We have assumed that the reddening is negligible, as the stars are all

nearby. A theoretical isochrone is used to estimate the stellar mass and the bolometric correction (BC) from the absolute M_v magnitude³, and they are combined with the *Hipparcos* parallax and the effective temperature to get the stellar gravity. The derived gravities are not very sensitive to errors in the assumed parameters. Thus, an error of 3% in T_{eff} typically produces uncertainties in the derived $\log g$ of 0.05 dex, a 30 % error in the mass translates to 0.13 dex, and an error of 30 % in the bolometric correction to a 0.05 dex error in the $\log g$. Nissen et al. (1997) have already argued that statistical biases in the parallaxes in a sample of this kind are unlikely to occur. We comment more on errors below.

We have collected data for F-K stars nearby stars (see below) from Bonnell & Bell (1993): 4 stars; Edvardsson (1988): 7 stars; Fuhrmann et al. (1997): 9 stars; Gratton et al. (1996): 214 stars; Magain (1989): 8 stars; and Ryan, Norris & Beers (1996): 1 star. In some of these works the spectroscopic gravities were derived from both the ionization balance and the wings of strong lines. These two criteria are known to differ (Edvardsson 1988, Fuhrmann 1998a) and we have first restricted the comparison to the ionization equilibrium gravities, which has been the procedure most extensively used. Bonnell & Bell (1993) derived gravities from the comparison of atomic and molecular magnesium features, but they also estimate and compile iron ionization balance gravities from the literature, which we discuss here.

Most of the data come from Gratton et al. (1996) who reanalyzed in a consistent fashion stars for which adequate and reliable data exist in the literature. Stellar effective temperatures were estimated afresh by Gratton et al. using the Infrared Flux Method

³No extrapolation was accepted here, and a star was excluded from the study when its mass and BC could not be obtained by interpolation in the theoretical isochrone of the metallicity assigned.

(Blackwell & Lynas-Gray 1994) while the gravities were obtained from the ionization equilibrium of iron. For their analysis, Gratton et al. use the Kurucz (1992) model atmospheres. The combined sample totals more than 300 stars with metallicities from $[\text{Fe}/\text{H}] \sim -3$ to ~ 0.2 . We shall not go deeper into details on the different effective temperature scales, model atmospheres, etc., employed by the different sources at this point. Several stars are common to two or more of these references and, in some cases, the discrepancies are large.

We have taken the published effective temperatures and derived the trigonometric gravities for those stars for which the *Hipparcos* parallax exceeds 10 mas^4 . Perryman et al. (1995) showed that the error of the parallax is typically less than 20% in such cases. Oxygen-enhanced isochrones by Bergbusch & Vandenberg (1992) were used within the published range, i.e. $-2.26 \leq [\text{Fe}/\text{H}] \leq -0.47$. For the stars falling outside this range, the appropriate extreme value was used. An age of 8 Gyr. was assumed for stars with $[\text{Fe}/\text{H}] > -0.47$. while an age of 12 Gyr. was adopted for those with $[\text{Fe}/\text{H}] \leq -0.47$. In principle, an individual determination of age and mass is possible with the present data, but the more schematic approach chosen here was found to be adequate because reducing the age assumed for the metal-poor stars from 12 Gyr. to 8 Gyr. increases the derived gravities by less than 0.06 dex for most of the stars. Alternative and likely improved isochrones have been published, but adopting those would have little effect on the derived trigonometric gravities, as we discuss below. In particular, newer calculations use the improved OPAL opacities (Iglesias et al. 1992), as those, e.g., by Bertelli et al. (1994). We find that use of Bertelli’s isochrones, which do not take α -elements enhancement for metal-poor stars into account, results in very small changes to the derived gravities, always below 0.1 dex.

The distribution of relative errors in the parallaxes of the sample, $\frac{\sigma}{\pi}$, is shown in Fig.

⁴miliarcseconds.

1. Most stars have relative errors in the parallax below 5%. Supposing that errors in the different quantities included in Equation 1 are independent from each other, we find

$$\sigma^2(\log g) = \log^2 e \left[\left(\frac{\sigma(M/M_\odot)}{M/M_\odot} \right)^2 + 16 \left(\frac{\sigma(T_{\text{eff}})}{T_{\text{eff}}} \right)^2 + 4 \left(\frac{\sigma(\pi)}{\pi} \right)^2 + 0.16 \left(\frac{\sigma(F_V)}{F_V} \right)^2 + 0.16 \left(\frac{\sigma(F_{BC})}{F_{BC}} \right)^2 \right] \quad (2)$$

where F_V and F_{BC} are the fluxes in and out the V band, respectively, and then, assuming errors in the stellar mass are of the order of 10%, the typical uncertainties in T_{eff} of $\sim 3\%$, those in the V photometric band and the bolometric corrections of about 5%, the derived $\log g$ will have an uncertainty of 0.08 dex. For the case $\frac{\sigma}{\pi} \simeq 0.08$, the uncertainty of the $\log g$ will be $\simeq 0.10$ dex.

The included stars, listed in Table 1, are shown in Figure 2 where we also plot representative theoretical isochrones. Metal-poor stars are shown by the filled circles ($[\text{Fe}/\text{H}] \leq -0.47$), while the open circles correspond to those richer than $[\text{Fe}/\text{H}] = -0.47$. Some stars have multiple entries in Table 1 and all figures, as they have been analyzed in more than one of the included references. There are also some stars that have multiple entries in the work of Gratton et al. (1996), corresponding to the different sources they took the equivalent widths from. Nissen et al. (1997) found that a shift of 100 K in the effective temperature of the isochrones was needed to match their sample of stars to the isochrones, and pointed out that the shift is equivalent to a decrease of the convection parameter α to a value less than unity. From the inspection of Fig. 2, we cannot conclude whether a shift is needed or not for the present sample. (The temperature scale of Gratton et al. 1996 has been used for most of the stars and in fact, Gratton et al. have shown that there are important systematic discrepancies between their T_{eff} scale and that of Edvardsson et al. 1993 and Nissen et al. 1994). A detailed comparison shows that there are systematic and much more complicated deviations than a constant shift between the T_{eff} s used here (see

Table 1) and those included in the isochrones.

Results from the compiled sample are first shown in Figure 3 where we plot $\log g$ from spectroscopy versus $\log g$ from the trigonometric parallaxes for a metal-poor and a metal-rich sample, where $[\text{Fe}/\text{H}] = -0.47$ is again taken as the boundary between both. At first glance, there are not large differences between the spectroscopic (iron ionization) and trigonometric gravities: the mean difference between the two gravity estimates is $\Delta \log g = 0.08 \pm 0.21$ (1σ) dex. Although this value has been drawn combining data from different sources, the comparison source by source reflects that the scatter is not greatly reduced (see Table 2). If the spectroscopic gravities are correct to 0.15 dex, and the trigonometric estimates have errors of 0.08 dex (as previously estimated for most of the stars studied here), the rms difference should be about 0.17 dex, in agreement with the results for the individual works in Table 2 (0.15 dex–0.25 dex). Systematic deviations between the spectroscopic gravities derived from different groups arising from the use of different effective temperature scales, atomic data, model atmospheres, etc. account well for the rms difference for the compiled sample (0.21 dex). It is apparent from Fig. 3 that the metal-poor stars show the largest deviations, and a clear correlation can be seen in Table 2 between the mean metallicity of the subsamples and the mean of deviations of the spectroscopic gravities from the trigonometric values. This is studied in detail in the next section.

3. The effect of the metallicity on the spectroscopic gravities.

The overall agreement, within the expected errors, between the spectroscopic and the trigonometric gravities found in the previous section can be analyzed in more detail by looking for dependences of the discrepancies on the stellar properties. The different works combined in this analysis correspond in some cases to small (this does not apply to

Gratton et al. 1996, which includes more than 200 nearby stars), homogeneous samples of stars, such as the metal-rich giants in Bonnell & Bell (1993) and Edvardsson (1988), or the metal-poor stars analyzed by Magain (1989) and Fuhrmann et al. (1997). Combining all these studies, we provide a general perspective by covering a larger zone in the space of the stellar parameters. Nevertheless, special care has to be taken, as systematic effects may be present among the different subsamples.

Figure 4a shows the differences found in Section 2 as a function of the stars’ effective temperature and gravity, while Fig. 4b displays the same differences against metallicity. The different subsamples are identified with distinct symbols. While no correlation is present between the discrepancies and the gravity or the effective temperature, a trend with metallicity is apparent. However, metal-poor stars belong mainly to the galactic halo, in opposition to more metal-rich stars which correspond to the disk –in a very simplified picture–, and hence they tend to be more rarely present in the solar vicinity (not very far from the galactic plane) than solar-metallicity stars. This makes the metal-poor stars in the sample tend to be at larger distances and therefore, the relative errors in their parallaxes are larger than those for metal-rich stars. Fig. 5 (top panel) shows this effect. Restricting the analysis to the stars with uncertainties in the parallax between 5 % and 10 % eliminates the systematic biases, as confirmed by the histogram in the middle panel of Fig. 5, but the trend of $\log g(\text{Spec.}) - \log g(\text{Trig.})$ with the metallicity seen in Fig. 4b persists (see Fig. 5, lower panel).

The question of whether systematic effects in the trigonometric gravities may arise from the stellar evolutionary models and the assumed stellar ages can be addressed by repeating the calculations using a different set of models. The upper panel in Fig. 6 shows the differences between the gravities derived using the isochrones of Bertelli et al. (1994) and those of Bergbusch & Vandenberg (1992). Again, the nearest extreme metallicity in

the published grid was employed for the stars outside the metallicity range of the models ($-1.7 < [\text{Fe}/\text{H}] < 0.4$ for Bertelli et al). The lower panel reflects the differences in the gravities when assuming the same metallicity for all stars ($[\text{Fe}/\text{H}]=-0.47$) and the same age (12 Gyrs.), making use of Bergbusch & Vandenberg’s isochrones. These differences cannot account for the systematic effects shown in Fig. 4b for stars more metal-poor than $[\text{Fe}/\text{H}]=-1.0$.

3.1. $[\text{Fe}/\text{H}] > -1$

This sample of stars is strongly dominated by the data from Gratton et al. (1996). The stars analyzed by Bonnell & Bell (1993) and Edvardsson (1988) have been introduced here to expand the sample of stars with large gravities (see Fig. 4a, upper panel).

The mean difference between the spectroscopic and the trigonometric gravities is 0.10 ± 0.17 (1σ) dex, and a linear regression analysis confirms the visual impression from Fig. 7a in the sense that none of the subsamples exhibits a statistically significant slope of the gravity discrepancy with metallicity. We note that the rms deviation is in agreement with our expectations, as described in §2, assuming the spectroscopic values have errors of 0.15 dex.

3.2. $[\text{Fe}/\text{H}] \leq -1$

Fig. 7b differs from an expansion of Fig. 4b in that the stars of Magain (1989) have been shifted in metallicity by +0.17 dex to take into account that his analysis was not differential to the Sun and, in contrast to Fuhrmann et al. (1997) and Gratton et al. (1996), he assumed the solar iron abundance to be significantly larger than the meteoritic value, in particular $\log N(\text{Fe})_{\odot} + 12 = 7.68$.

A clear zero-point shift exists between the spectroscopic (iron ionization balance) gravities of Gratton et al. and those derived by Fuhrmann et al. and Magain. Magain and Gratton et al. use laboratory transition probabilities whenever possible, supplemented with *solar* empirical data obtained with the help of the Holweger & Müller (1974) model photosphere. Despite the use of different model atmospheres, the systematic discrepancy between them can largely be ascribed to their effective temperature scales: the T_{eff} s assigned by Magain for the 16 stars in common are cooler by -136 ± 24 K than those of Gratton et al. Ionization balance establishes that $\Delta \log g \simeq 0.002 \times \Delta T_{\text{eff}}$ (see, e.g., Allende Prieto 1998, Fig. 1.2), or $\Delta \log g \simeq 0.005 \times \Delta T_{\text{eff}}$ (following the considerations in §5) thus the offset in the temperature scale accounts for the displacement observed in the spectroscopic gravities. The same explanation does not apply to the discrepancy between Gratton et al. and Fuhrmann, already discussed by Fuhrmann (1998a). Their T_{eff} scales, based on the wings of the Balmer lines (Fuhrmann) and the Infra-Red Flux Method (Gratton et al.), are consistent for metal-poor stars (Gratton et al. 1996, Fuhrmann 1998a). In particular, the 4 stars in common included in Table 1 show a mean difference of 8 ± 50 K. Several elements in the analyses are different and may be acting to induce the divergence between the gravity scales, placing Fuhrmann’s results closer to those of Magain: model atmospheres, transition probabilities, and equivalent widths.

Setting aside systematic shifts in the gravity scales, our three sources show the spectroscopic gravities to become smaller relative to the trigonometric estimates towards lower metallicities. The slopes of a linear model ($\Delta \log g = a \times [\text{Fe}/\text{H}] + b$), obtained by minimizing the χ^2 statistics, are consistent for the three references: $a = 0.33 \pm 0.08$ (Gratton et al.), 0.33 ± 0.06 (Fuhrmann), and 0.41 ± 0.16 (Magain). The spectroscopic gravity found by Ryan et al. (1996) for HD140283 lies in between those found by Fuhrmann (or Magain) and Gratton et al. The positive slope of the gravity discrepancies raises the question of whether this trend will continue towards lower values, producing important (metallicity

dependent) errors in the spectroscopic gravities for the stars in the domain $[\text{Fe}/\text{H}] \leq -3$. This would affect to the conclusions extracted from analyses of chemical abundances in extremely metal-poor stars that make use of the ionization equilibrium to derive the surface gravity. Unfortunately, such halo stars are too distant for an accurate determination of their parallaxes.

To make sure that multivariate correlations are not masking real dependencies of the differences between spectroscopic and trigonometric gravities for metal-poor stars, we have corrected the trend with metallicity found for the sample of Gratton et al. and check for correlations with the other parameters, namely $\log g$ and T_{eff} . The result is again negative, as no trend is apparent.

Other consistency checks of the spectroscopic gravities have been performed for giants in globular clusters such as M15 (Snedden et al. 1997) and NGC7006 (Kraft et al. 1998), using the absolute magnitude of RR Lyr stars to estimate the distance to the cluster. The tests showed agreement within the expected uncertainties: $\sigma \simeq 0.15$ dex demonstrating that well evolved stars of moderately low metallicity, which are not represented in our sample, fit in the general picture of Fig. 4. Recently, evidence has accumulated for a brighter luminosity scale for the globular clusters (see, e.g., Reid 1997; Kovács & Walker 1999). This would make the physical gravities to be up to 0.2 dex lower than previously though, but still consistent with Fig. 4b.

4. Ionization vs. strong-line gravities.

The sensitivity of the wings of strong neutral metal lines to atmospheric pressure has been employed by many analysts to estimate surface gravities, as an alternative to the ionization balance. Among the spectroscopic studies compiled here, those of Edvardsson

(1988) and Fuhrmann et al. (1997)⁵ make use of this approach. Fuhrmann (1998a) has found a good agreement between the ionization balance and the strong-line gravities for stars of about the effective temperature of the Sun, but he argues in favor of the strong-line values for hotter stars, as the ionization equilibrium might be affected from NLTE effects and he indeed detects significant differences between the two methods for the hotter stars in his sample. The eight stars with $T_{\text{eff}} > 5900$ K whose gravities were determined using the ionization equilibrium (Fuhrmann et al. 1997), and from the analysis of Mg I strong lines by Fuhrmann (1998a) show that the strong-line gravities are preferred. This is shown in Fig. 8. The ionization balance gravities (filled circles) depart from the trigonometric values in -0.20 ± 0.12 (1σ) dex, while the strong-line gravities (open circles) get closer, dropping the difference down to -0.01 ± 0.13 dex. Regrettably, Edvardsson’s analysis of metal-rich evolved stars shows a different picture. Ionization equilibrium gravities for the seven stars compared here show a mean difference with the trigonometric gravities of $+0.19 \pm 0.15$ dex, while the strong-line method leads to larger departures, providing a mean of $+0.50 \pm 0.17$ dex.

The discrepant results may arise from different elements in the analysis (model atmospheres, atomic data, damping treatment, etc.) or may emerge naturally from differences in temperature and gravity covered by the samples. Edvardsson used the T_{eff} scale of Frisk (1983), which was built upon flux-constant model photospheres. There is no simple way of making a meaningful comparison between Frisk’s and Fuhrmann’s temperature scales. We can only conclude that strong-line gravities are systematically larger than those derived from the ionization balance by 0.2–0.3 dex, and they are a better estimate for dwarf and subgiants with $\log g > 3.5$ when derived in the scale of Fuhrmann.

The applicability of the strong-line method to metal-poor stars becomes more difficult

⁵Updated from Fuhrmann (1998a) for the stars analyzed here.

when the metallicity drops, as the wings of the lines become less prominent. For the extreme metal-poor stars with $[\text{Fe}/\text{H}] < -3$, it is doubtful that any useful result can be drawn from this method (Fuhrmann 1998b).

5. The connection between departures from the excitation equilibrium and the ionization balance.

We mentioned in the introduction that Magain & Zhao (1996) found strong departures from the excitation equilibrium for neutral iron lines in metal-poor stars. They presented a complicated picture in which the iron abundances derived from high and low excitation lines differ by up to +0.3 dex for the hotter stars in their sample ($T_{\text{eff}} \sim 6000\text{--}6200$ K). The estimates from high excitation lines were generally larger for almost all the studied stars, in particular for the stars in the turnoff.

If such a discrepancy is present, it will affect significantly the gravities derived through the ionization equilibrium. Assuming the continuum as shaped by the H^- bound-free opacity, for an element which is mostly ionized (as it is the case for iron in solar-like stars), we expect the abundances derived from neutral lines to have a dependence with temperature of -1.3×10^{-3} dex/K when the excitation potential (χ) is about 0 eV and -0.4×10^{-3} dex/K when χ is about 5 eV (see Gray 1992, pages 286–287). Therefore, a discrepancy of +0.3 dex between high excitation and low excitation lines correspond to a systematic deviation in the derived mean abundance of roughly -0.3 dex compared with the result that would be obtained when the excitation balance is accomplished. Approximating the dependence of the electron pressure on the star’s gravity as $P_e \propto g^{\frac{1}{3}}$, the ratio of the line to continuum opacities for a Fe II line is expected to be $\frac{\kappa_{\nu}}{\chi_{\nu}} \propto g^{-\frac{1}{3}}$ (Gray 1992; pages 287–290) and then, as the line opacity is also proportional to the abundance $N(\text{Fe})$, the product $N(\text{Fe}) g^{-\frac{1}{3}}$ remains constant for a given line equivalent width. In this situation, we can estimate

errors in the ionization balance gravities induced by errors in the abundance derived from Fe I lines as $\Delta(\log g) = 3 \times \Delta [\text{Fe}/\text{H}]$. This has been illustrated in Fig. 9 for the sake of clarity. We are allowed then to translate the -0.3 dex error in the iron abundance to a systematic deviation of -0.9 dex in the iron ionization gravities, which is close to the discrepancies in Fig. 7 for the more metal-poor stars in the samples of Fuhrmann et al. (1997) and Magain (1989).

HD140283 is probably the most metal-poor star in this study, and it has been analyzed by four different sources. Magain (1989) derived photometrically (neglecting the reddening) $T_{\text{eff}} = 5640$ K for this star, and then $\log g = 3.1$ dex from the iron ionization equilibrium. If this star fits in the general panorama for departures from excitation equilibrium described by Magain & Zhao (1996; their Fig. 4), they would have found a discrepancy of $\sim +0.1$ dex between the iron abundances derived from high and low-excitation potential lines. The higher effective temperature (+110 K) employed by Ryan et al. (1996) will help to achieve the Fe I excitation balance, and will result in a larger gravity (also metallicity), as is indeed the case: $\log g = 3.4$ dex. The even slightly hotter T_{eff} (between +115 and +139 K) of Gratton et al. (1996) might overcorrect for the effect, as confirmed by the small but *negative* slope of Fe I abundances with excitation potential they found for a selection of stars. Nonetheless, we cannot explain the low spectroscopic (iron ionization) gravity found by Fuhrmann et al. (1997), $\log g = 3.2$ (in agreement with Magain 1989), as they assign to the star a much higher T_{eff} ($\sim +200$ K), but we note that their f -values have been estimated from the analysis of the solar flux spectrum with a flux-constant model atmosphere, in opposition to the general rule followed by Magain, Gratton et al., and Ryan et al., who use laboratory data whenever possible.

We conclude that it is possible, if not likely, that the observed departures from the excitation equilibrium in neutral iron lines are connected with the discrepancies reported

here between iron ionization gravities and the trigonometric estimates. The physical origin of both has to be investigated, and several paths to follow are suggested in the next section.

6. Conclusions and suggestions for future work.

The comparison of spectroscopic measurements and synthetic spectra can be used to constrain what the fundamental parameters characterizing a star should be. When one of these parameters can be reliably measured through another means, it can be used to carry out a consistency check, testing the adequacy of the modeling. Unfortunately, direct measurement of fundamental stellar parameters, such as the radius, or the mass, is rarely possible, especially for isolated stars. Additionally, it is particularly difficult to determine the distance to the star, which is needed to derive other basic properties, such as the luminosity.

Measurements of stellar parallaxes provide distance estimates for a set of nearby stars that has been significantly enlarged with the recent release of the *Hipparcos* mission data. Here, we have derived the distances for late-type stars with highly accurate *Hipparcos* parallaxes and which had been the subject of high-resolution spectroscopic analysis in the literature. The parallaxes with the V magnitude provide the absolute magnitude M_v which, combined with models of stellar evolution and an estimate of the effective temperature, gives a fairly accurate determination of the gravity. The comparison of these *trigonometric* gravities with those derived from published spectroscopic analyses (ionization balance), assuming the same effective temperatures, reveals:

- good agreement for stars in the metallicity range $-1.0 < [\text{Fe}/\text{H}] < 0.3$, the mean difference being $< \log g (\text{Spec.}) - \log g (\text{Trig.}) > = +0.10 \pm 0.17 (1\sigma)$ dex, consistent with a scatter in the spectroscopic (iron ionization balance) gravities of 0.15 dex.

- a larger discrepancy for stars with metallicities below $[\text{Fe}/\text{H}] = -1$. The discrepancy increases towards lower metallicities, as suggested by three independent sources for the spectroscopic gravities.

These findings cast a shadow upon analyses of extreme metal-poor stars based on gravities derived from the ionization balance, until independent estimates of the stellar fundamental properties can be obtained. Future astrometric missions, such as SIM (Unwin, Yu & Shao 1997) or GAIA (Lindegren & Perryman 1997) will push the accuracy of the parallaxes down to the level of a few microarcseconds, and reach stars as faint as $V=15$.

Our discussion cannot cover metal-poor low-gravity stars, as they are not represented in the studied sample. However, we note that a similar consistency check that involves the absolute brightness of RR Lyr variables as an independent distance estimate, has been satisfactorily applied to giants in the globular clusters M15 (Snedden et al. 1997) and NGC7006 (Kraft et al. 1998).

A comparison of the strong-line gravities derived by Edvardsson (1988) and Fuhrmann (1988a) confirms that this method provide systematically larger gravities. However, while the strong-line gravities get closer to the physical ones for the stars in or near the turnoff, they are even further away than the iron ionization gravities for the low-gravity stars analyzed by Edvardsson (1988). The origin of these systematic differences remains unclear. We remark that this method cannot be applied to extreme metal-poor stars, as the wings of the lines lose their sensitivity to pressure.

Some of the published claims on departures from the iron excitation equilibrium in metal-poor stars appear to be connected with the discrepancies found here between spectroscopic (iron ionization) and trigonometric gravities.

Several factors influence the spectroscopically derived gravities and are capable of

producing systematic deviations, namely, the scale of effective temperatures, the treatment of the line damping, the atomic data, and other ingredients involved in the modeling, as well as the measurement error itself. Departures from LTE are expected to make the spectroscopic gravities to diverge further from the physical ones when the metallicity gets lower. Very recently, Thévenin & Idiart (1999) have explored this possibility in detail. Using complex atomic models for neutral and ionized iron and photoionization cross-sections from the Iron Project (Bautista 1997), they have studied departures from LTE in the line formation for a sample of stars in the range $-4 \leq [\text{Fe}/\text{H}] \leq 0$, concluding that they exist and become significantly larger towards lower metallicities as a result of iron overionization compared to LTE predictions. In Fig. 10, we overplotted their corrections to the LTE gravities (filled stars; from their Table 1) on top of our Fig. 4b, as well as a least-squares quadratic fit to their data (solid line). Constrasting of Gratton et al.’s data (filled circles) with the corrections of Thévenin & Idiart suggests that NLTE in the line formation is not the unique element at work, and something else is distorting further the gravity estimates. Nevertheless, a very different perspective emerges when the sample of Gratton et al. is excluded from the comparison. In that case, a quadratic polynomial fit to the observed discrepancies (dashed line) will be roughly consistent with the departures from LTE predicted by Thévenin & Idiart.

Definitely, NLTE in the line formation may explain the discrepancies between spectroscopic and trigonometric gravities for metal-poor dwarfs at about $[\text{Fe}/\text{H}] \sim -2.5$. Additional effects might present, as suggested by the fact that the slope of the discrepancies between LTE iron ionization and the trigonometric gravities for stars more metal-poor than $[\text{Fe}/\text{H}]=-1$ is steeper ($\sim +0.35$; see §3.2) than Thévenin & Idiart’s predictions ($+0.06$). This conclusion is independently reached using either the sample of Gratton et al., Fuhrmann et al., or Magain. NLTE effects could be important when modeling the atmospheres of metal-poor stars. Hauschildt, Allard, & Baron (1999) have computed

flux-constant model atmospheres in NLTE for Vega and the Sun. An extension of these computations to metal-poor stars is desirable to test for departures from LTE that induce deviations from the ionization and excitation balance. Besides, we cannot exclude the effect of atmospheric inhomogeneities on the line formation as a factor inducing the observed discrepancies. Allende Prieto et al. (1995, 1999) compared convective line asymmetries in the metal-poor star HD140283 with the solar case, finding significantly larger velocities for the metal deficient star. Detailed three dimensional hydrodynamical simulations of surface convection in metal-poor stars (Asplund et al. 1999) should provide tremendous insight on such a controversial issue.

We still have to emphasize that systematic effects between different analyses are large. This reveals inadequate implementations of the methods employed in the spectroscopic studies. These artificial systematic deviations must be reduced to search for and clarify possible failures either in the physical assumptions or in the model atmospheres.

We thank the anonymous referee for many useful comments and suggestions. This work has been partially funded by the Spanish DGES under projects PB92-0434-C02-01 and PB95-1132-C02-01, the U.S. National Science Foundation (grant AST961814), and the Robert A. Welch Foundation of Houston, Texas. We have made use of data from the *Hipparcos* astrometric mission of the ESA, and the NASA ADS.

REFERENCES

- Allende Prieto, C., 1998, Surface Inhomogeneities and Semi-Empirical Modeling of Metal-Poor Stellar Photospheres, PhD Thesis (La Laguna: IAC)
- Allende Prieto, C. , García López, R. J., Lambert, D. L., & Gustafsson, B. 1995, in Stellar Surface Structure, IAU Symp. 176: Poster Proceedings, ed. K. G. Strassmeier (Vienna: Institut für Astronomie der Universität Wien), 107
- Allende Prieto, C. , García López, R. J., Lambert, D. L., & Gustafsson, B. 1999, ApJ, in press
- Asplund, M., Nordlund, Å, Trampedach, R., & Stein, R. F. 1999, A&A, 346, L17
- Bautista, M. A. 1997, A&AS, 122, 167
- Bell, R. A., & Oke, J. B. 1986, ApJ, 307, 253
- Bergbusch, P. A., & Vandenberg, D. A. 1992, ApJS, 81, 163
- Bertelli, G., Bressan, A., Chiosi, C., Fagotto, F., & Nasi, E. 1994, A&AS, 106, 275
- Blackwell, D. E., & Lynas-Gray, A. E. 1994, A&A, 282, 899
- Bonnell, J. T., & Bell, R. A. 1993, MNRAS, 264, 334
- Castelli, F., Gratton, R. G., & Kurucz, R. L. 1997, A&A, 318, 841
- Dalle Ore, C. M. 1993, PhD Thesis, University of California at Santa Cruz
- Dommanget, J., & Nys O. 1994, Comm. Obs. R. Belgique, Ser. A, N. 115
- Edvardsson, B. 1988, A&A, 190, 148
- Edvardsson, B., Andersen, J., Gustafsson, B., Lambert, D. L., Nissen, P. E., & Tomkin, J. 1993, A&A, 275, 101
- ESA 1997, The Hipparcos and Tycho Catalogues, ESA SP-1200
- Frisk, U. O. 1983, Stockholm Observatory Report No. 23

- Fuhrmann, K. 1998a, *A&A*, 338, 161
- Fuhrmann, K. 1998b, *A&A*, 330, 626
- Fuhrmann, K., Axer, M., & Gehren, T. 1993, *A&A*, 271, 451
- Fuhrmann, K., Pfeiffer, M., Frank, C., Reetz, J., & Gehren, T. 1997, *A&A*, 323, 909
- Gratton, R. G., Carretta, E., & Castelli, F. 1996, *A&A*, 314, 191
- Gray, D. F. 1992, *The Observation and Analysis of Stellar Photospheres* (Cambridge: Cambridge University Press)
- Gustafsson, B., & Bell, R. A. 1979, *A&A*, 74, 313
- Gustafsson, B., & Jørgensen, U. G. 1994, *A&A Rev.*, 6, 19
- Hauschildt, P. H., Allard, F., & Baron E. 1999, *ApJ*, 512, 377
- Holweger, H., & Müller, E. A. 1974, *Solar Phys.*, 39, 19
- Iglesias, C. A., Rogers, F. J., & Wilson, B. G. 1992, *ApJ*, 397, 717
- Kovács, G., & Walker, A. R. 1999, *ApJ*, 512, 271
- Kraft, R. P., Sneden, C., Smith, G. H., Shetrone, M. D., & Fulbright, J. 1998, *AJ*, 115, 1500
- Kurucz, R. L. 1992, private communication
- Lindgren, L., & Perryman, M. A. C. 1997, The first results of the Hipparcos and Tycho, 23rd meeting of the IAU, Joint Discussion 14, 25 August 1997, Kyoto, Japan
- Magain, P. 1984, *A&A*, 132, 208
- Magain, P. 1985, *A&A*, 146, 95
- Magain, P. 1987, *A&A*, 181, 323
- Magain, P. 1989, *A&A*, 209, 211
- Magain, P., & Zhao, G. 1996, *A&A*, 305, 245

- Nissen, P. E., Gustafsson B., Edvardsson B., Gilmore, G. 1994, *A&A*, 285, 440
- Nissen, P. E., Høg, E., & Schuster, W. J. 1997, *Proceedings of the ESA Symposium Hipparcos - Venice '97*, ESA SP-402 (Venice: ESA), 225
- Perryman, M. A. C., Lindegren, L., Kovalevsky, J., Turon, C., Høg, E., Grenon, M., Schrijver, H., Bernacca, P. L., Creze, M., Donati, F., Evans, D. W., Falin, J. L., Froeschle, M., Gomez, A., Grewing, M., Van Leeuwen, F., Van der Marel, J., Mignard, F., Murray, C. A., Penston, M. J., Petersen, C. S., Le Poole, R. S., & Walter, H. 1995, *A&A*, 304, 69
- Reid, I. N. 1997, *ApJ*, 114, 161
- Ryan, S. G., Norris, J. E., & Beers, T. C. 1996, *ApJ*, 471, 254
- Snedden, C., Kraft, R. P., Shetrone, M. D., Smith, G. H., Langer, G. E., & Prosser, C. F. 1997, *AJ*, 114, 1964 M. Jaschek & P. C. Keenan, eds., (Dordrecht: Reidel), 231
- Steffen, M. 1985, *A&A*, 59, 403
- Thévenin, F., & Idiart, I. P. 1999, *ApJ*, in press
- Unwin, S. C., Yu, J. W., & Shao, M. 1997, *BAAS*, 191, 23.02
- Van't Veer-Menneret, C., & Megessier, C. 1996, *A&A*, 309, 879
- Vandenberg, D. A. 1985, *ApJS*, 58, 56

Fig. 1.— Distribution of the nominal relative errors in the *Hipparcos* parallaxes for the program stars.

Fig. 2.— The $T_{\text{eff}} - M_v$ diagram. Selected isochrones from Vandenberg (1985; solar metallicity) and Bergbusch & Vandenberg (1992; metal-poor) are drawn. Stars from Table 1 are plotted. Filled circles represent stars of $[\text{Fe}/\text{H}] \leq -0.47$, while open circles represent stars with $[\text{Fe}/\text{H}] > -0.47$.

Fig. 3.— Comparison of spectroscopic and trigonometric gravities. Metal-rich stars ($[\text{Fe}/\text{H}] > -0.47$) are indicated with filled circles and metal-poor stars are with open circles. The solid line corresponds to the case $\log g$ (spectroscopic) = $\log g$ (trigonometric).

Fig. 4.— a) The differences between spectroscopic and trigonometric gravities are plotted as a function of the trigonometric gravity and the effective temperature. The different symbols identify the different sources for the spectroscopic data: Gratton et al. (1996; filled circles), Edvardsson (1988; asterisks), Bonnell & Bell (1993; pluses), Fuhrmann et al. (1997; rhombi), Magain (1989; squares), and Ryan et al. (1996; cross); b) Differences between spectroscopic and trigonometric gravities against the iron abundance.

Fig. 5.— Correlation between the relative errors in the parallaxes and the stellar iron abundance (upper panel). Histogram of the metallicity distribution for the stars with relative errors $0.05 \leq \sigma(\pi)/\pi \leq 0.10$ (mid panel). Differences between spectroscopic and trigonometric gravities for the stars with relative errors $0.05 \leq \sigma(\pi)/\pi \leq 0.10$ (lower panel). The symbols follow the same code explained in Fig. 4.

Fig. 6.— Differences between the trigonometric gravities derived from: Bertelli et al. (1994) or Bergbusch & Vandenberg (1992) (upper panel), and Bergbusch & Vandenberg (1992) assuming all the stars have $[\text{Fe}/\text{H}] = -0.47$ or taking their real metallicities into account to estimate their masses and bolometric corrections (lower panel). Note that the

(OPAL) Bertelli et al’s isochrones cover the range $-1.7 < [\text{Fe}/\text{H}] < 0.4$, while Bergbush & Vandenberg’s (O-enhanced) models span the metallicity band $-2.3 < [\text{Fe}/\text{H}] < -0.4$. The extreme values were applied when the metallicity exceeded the limits.

Fig. 7.— Differences between the spectroscopic (iron ionization) gravities and the trigonometric estimates as a function of the stellar metallicity in the ranges $-1.0 < [\text{Fe}/\text{H}] < 0.3$ (a) and $-2.6 < [\text{Fe}/\text{H}] < -1.0$ (b). The metallicities given by Magain (1989) have been shifted by $+0.17$ to take into account that he adopted a higher solar abundance than the (\sim meteoritic) value used by the others. The solid lines show χ^2 -linear fits to the data for each reference.

Fig. 8.— The strong-line gravities (open circles) and the iron ionization gravities (filled circles) are compared with the *Hipparcos* trigonometric gravities. Symbols in the upper right part of the plot correspond to the spectroscopic analysis of Fuhrmann et al. (1997) and Fuhrmann (1998), while those in the bottom left correspond to the study of Edvardsson (1988).

Fig. 9.— The figure illustrates the behavior of the abundances derived from neutral iron lines (left panel) and singly ionized iron lines (right panel) in a solar-like photosphere. Besides, the arrows indicate the connection between departures in the excitation balance and those in the ionization equilibrium.

Fig. 10.— Differences between spectroscopic and trigonometric gravities against the iron abundance. The different symbols identify the various sources for the spectroscopic data and are the same used in previous figures (e.g. Fig. 4). The stars show the NLTE corrections to the ionization equilibrium gravities calculated by Thévenin & Idiart (1999). The solid and dashed lines correspond to least-square polynomial fits to the corrections of Thévenin & Idiart and the differences $\log g(\text{Spec.}) - \log g(\text{Trig.})$ (excluding Gratton et al’s data),

respectively.

Table 1. Data for the stars in the comparison

Star	[Fe/H]	Mass M_{\odot}	V	M_v	T_{eff} K	log g Hipparcos	log g Spectroscopic	π mas	$\sigma(\pi)$ mas	Ref. ^a	Iso. ^b	CCDM ^c
HR 17	-0.34	1.01	6.21	3.61	6168	4.09	4.07	30.26	0.69	0	1	
HR 33	-0.37	1.02	4.89	3.51	6193	4.06	4.16	52.94	0.77	0	1	
HR 35	-0.14	1.02	5.24	3.55	6491	4.15	4.30	45.85	0.66	0	1	
HR 107	-0.37	1.04	6.05	3.25	6431	3.95	4.06	27.51	0.86	0	1	
HR 140	0.04	1.02	5.57	3.53	6437	4.13	4.42	39.03	0.62	0	1	
HR 145	-0.23	1.02	6.32	3.44	6178	4.03	3.93	26.59	0.85	0	1	
HR 203	-0.25	1.01	6.15	3.63	5793	3.99	4.12	31.39	1.03	0	1	00455-1253
HR 219	-0.31	0.92	3.46	4.59	5897	4.36	4.35	167.99	0.62	0	1	00491+5749
HR 235	-0.20	0.96	5.17	4.22	6168	4.31	4.53	64.69	1.03	0	1	
HR 244	-0.04	1.02	4.80	3.46	6105	4.01	4.10	53.85	0.60	0	1	00531+6107
HR 340	-0.13	1.05	5.67	2.06	5780	3.27	3.26	18.98	0.71	0	1	
HR 366	-0.33	1.04	5.14	3.20	6419	3.93	4.17	41.01	0.89	0	1	01144-0755
HR 370	0.09	0.98	4.97	4.08	5994	4.21	4.26	66.43	0.64	0	1	
HR 448	0.13	1.03	5.75	3.39	5804	3.90	3.80	33.71	0.72	0	1	
HR 458	0.06	1.02	4.10	3.45	6125	4.02	3.98	74.25	0.72	0	1	01367+4125
HR 483	-0.04	0.94	4.96	4.45	5825	4.29	4.33	79.09	0.83	0	1	
HR 573	-0.36	0.98	6.10	4.00	6206	4.24	4.12	37.97	0.61	0	1	
HR 646	-0.30	1.04	5.23	2.84	6334	3.75	3.94	33.19	0.85	0	1	
HR 672	0.02	1.01	5.60	3.61	5968	4.03	4.25	40.04	0.92	0	1	
HR 720	-0.18	1.02	5.89	3.45	5840	3.93	3.81	32.48	0.84	0	1	
HR 740	-0.24	1.04	4.74	2.68	6409	3.71	4.06	38.73	0.87	0	1	
HR 784	-0.01	0.97	5.79	4.12	6209	4.29	4.16	46.42	0.82	0	1	
HR 799	-0.04	1.00	4.10	3.85	6239	4.20	4.35	89.03	0.79	0	1	02441+4913
HR 962	0.07	1.04	5.07	3.32	6015	3.87	3.94	44.69	0.75	0	1	03128-0112
HR 1083	-0.14	1.04	4.71	3.05	6695	3.94	4.33	46.65	0.48	0	1	03294-6256
HR 1101	-0.11	1.01	4.29	3.60	5950	4.02	4.00	72.89	0.78	0	1	
HR 1173	0.01	1.04	4.22	2.95	6569	3.87	4.20	55.79	0.69	0	1	
HR 1257	0.03	1.04	5.36	2.66	6219	3.65	3.85	28.87	0.82	0	1	
HR 1294	-0.15	0.93	6.37	4.54	5727	4.29	4.28	43.12	0.50	0	1	
HR 1489	0.03	1.02	5.97	3.50	5942	3.98	4.01	32.03	0.91	0	1	
HR 1536	0.14	1.01	5.77	3.65	5807	4.00	3.98	37.73	0.89	0	1	
HR 1545	-0.37	1.02	6.27	3.53	6342	4.11	4.55	28.28	0.80	0	1	
HR 1673	-0.32	1.04	5.11	3.12	6397	3.89	4.00	39.99	0.70	0	1	
HR 1687	0.20	1.04	5.89	2.97	6456	3.84	4.02	26.04	0.83	0	1	
HR 1729	-0.04	0.97	4.69	4.18	5824	4.20	4.26	79.08	0.90	0	1	05192+4007
HR 1780	0.01	0.97	5.00	4.17	6108	4.27	4.07	68.19	0.94	0	1	05244+1723
HR 1907	-0.50	0.94	4.09	1.33	4720	2.55	2.30	28.10	0.91	2	0	
HR 1983	-0.12	1.00	3.59	3.83	6299	4.21	4.10	111.49	0.60	0	1	05445-2226
HR 2047	-0.04	0.91	4.39	4.70	5895	4.40	4.21	115.43	1.08	0	1	05544+2017
HR 2141	-0.24	0.98	6.12	4.01	5887	4.15	4.35	37.90	0.83	0	1	06061+3524
HR 2220	-0.01	1.01	5.20	3.58	6467	4.16	4.30	47.33	0.86	0	1	06148+1909
HR 2354	0.14	0.99	6.45	3.94	5739	4.08	4.10	31.46	0.52	0	1	
HR 2493	-0.37	0.95	6.43	4.31	6037	4.30	4.59	37.60	0.65	0	1	
HR 2548	-0.24	1.04	5.14	3.13	6386	3.89	4.14	39.66	0.53	0	1	
HR 2601	-0.50	0.94	6.20	2.82	6056	3.62	4.02	21.10	0.90	0	0	06588+2605
HR 2721	-0.27	0.94	5.54	4.41	5913	4.30	4.38	59.31	0.69	0	1	
HR 2835	-0.50	0.91	6.54	4.09	6227	4.25	4.30	32.43	0.91	0	0	

Table 1—Continued

Star	[Fe/H]	Mass M_{\odot}	V	M_v	T_{eff} K	log g Hipparcos	log g Spectroscopic	π mas	$\sigma(\pi)$ mas	Ref. ^a	Iso. ^b	CCDM ^c
HR 2883	-0.70	0.91	5.90	3.52	5994	3.90	4.15	33.40	0.93	0	0	07321-0853
HR 2906	-0.18	1.05	4.44	2.39	6149	3.52	3.75	38.91	0.66	0	1	
HR 2943	-0.06	1.04	0.40	2.68	6605	3.76	4.13	285.93	0.88	0	1	07393+0514
HR 3018	-0.72	0.86	5.36	4.45	5890	4.27	4.42	65.79	0.56	0	0	
HR 3018	-0.78	0.85	5.36	4.45	5723	4.22	4.21	65.79	0.56	0	0	
HR 3176	0.09	1.02	5.30	3.46	5728	3.90	3.84	42.86	0.97	0	1	
HR 3220	-0.29	1.04	4.74	3.09	6457	3.89	4.28	46.75	3.38	0	1	
HR 3262	-0.26	1.00	5.13	3.84	6301	4.21	4.11	55.17	0.93	0	1	
HR 3538	0.02	0.90	6.01	4.85	5687	4.38	4.37	58.50	0.88	0	1	
HR 3578	-0.76	0.87	5.80	4.16	5971	4.18	4.62	46.90	0.97	0	0	
HR 3648	-0.06	1.00	5.18	3.72	5830	4.03	3.93	51.12	0.72	0	1	09143+6125
HR 3775	-0.21	1.05	3.17	2.52	6296	3.61	3.80	74.15	0.74	0	1	09329+5141
HR 3881	0.07	1.00	5.08	3.75	5828	4.04	3.92	54.26	0.74	0	1	
HR 3951	0.11	0.93	5.37	4.50	5675	4.26	4.28	67.14	0.83	0	1	10010+3155
HR 3954	0.01	1.05	5.71	2.34	6292	3.53	3.84	21.15	0.72	0	1	
HR 4012	0.15	1.05	6.02	2.44	6023	3.50	3.64	19.27	0.89	0	1	
HR 4027	-0.01	0.99	6.46	3.93	5772	4.09	4.11	31.25	0.81	0	1	
HR 4039	-0.38	0.98	5.81	4.03	6143	4.23	4.54	44.01	0.75	0	1	10172+2306
HR 4067	0.14	1.04	5.73	2.78	6186	3.69	3.83	25.65	0.70	0	1	
HR 4150	-0.21	1.04	6.29	2.96	6465	3.84	4.05	21.60	0.75	0	1	
HR 4158	-0.24	1.00	5.71	3.76	6093	4.12	4.18	40.67	0.68	0	1	10365-1214
HR 4257	-0.01	1.05	3.78	1.42	5025	2.75	2.95	33.71	0.57	1	1	10535-5851
HR 4257	0.00	1.05	3.78	1.42	4870	2.70	3.01	33.71	0.57	2	1	10535-5851
HR 4277	0.00	0.96	5.03	4.29	5811	4.23	4.09	71.04	0.66	0	1	
HR 4285	-0.25	1.04	6.03	2.74	5853	3.58	3.74	21.98	0.75	0	1	11003+4255
HR 4287	0.14	1.05	4.08	0.44	4820	2.23	2.60	18.71	1.03	1	1	
HR 4395	-0.15	1.05	5.08	1.87	6525	3.40	3.63	22.80	0.84	0	1	
HR 4421	-0.51	0.93	5.83	3.24	6623	3.95	4.23	30.40	0.60	0	0	
HR 4529	0.16	1.04	6.24	3.09	5977	3.76	3.80	23.49	0.80	0	1	11484-1018
HR 4540	0.10	1.02	3.59	3.40	6065	3.98	4.06	91.74	0.77	0	1	11507+0146
HR 4657	-0.66	0.87	6.11	4.34	6267	4.34	4.60	44.34	1.01	0	0	12152-1019
HR 4688	0.19	1.04	6.38	2.90	6256	3.76	4.01	20.12	0.77	0	1	
HR 4734	0.12	0.97	6.25	4.12	5665	4.13	4.08	37.50	0.72	0	1	
HR 4767	-0.13	0.93	6.20	4.49	5998	4.35	4.37	45.58	0.62	0	1	
HR 4785	-0.19	0.92	4.24	4.63	5814	4.35	4.29	119.46	0.83	0	1	
HR 4845	-0.51	0.86	5.95	4.75	5868	4.38	4.15	57.57	0.64	0	0	
HR 4903	0.29	1.04	5.89	2.89	5880	3.65	3.78	25.17	0.76	0	1	
HR 4981	-0.20	1.05	5.04	2.48	6301	3.60	3.78	30.72	0.80	0	1	13120-1611
HR 4983	0.00	0.94	4.23	4.42	5952	4.32	4.31	109.23	0.72	0	1	13118+2753
HR 4989	-0.29	1.01	4.90	3.62	6263	4.12	4.32	55.49	0.65	0	1	13142-5906
HR 5011	0.10	0.99	5.19	3.92	5920	4.13	3.96	55.71	0.85	0	1	13168+0925
HR 5019	-0.03	0.87	4.74	5.09	5552	4.42	4.33	117.30	0.71	0	1	13185-1818
HR 5235	0.20	1.05	2.68	2.41	5943	3.47	3.38	88.17	0.75	0	1	13547+1824
HR 5287	0.12	1.05	3.25	0.79	4620	2.32	2.20	32.17	0.77	1	1	
HR 5323	0.03	1.04	5.53	2.92	6130	3.73	3.99	30.06	0.74	0	1	
HR 5338	-0.11	1.05	4.07	2.42	6127	3.52	3.71	46.74	0.87	0	1	
HR 5353	0.19	0.99	6.47	3.89	5483	3.99	3.90	30.47	1.00	0	1	14180-0732

Table 1—Continued

Star	[Fe/H]	Mass M_{\odot}	V	M_v	T_{eff} K	log g		π mas	$\sigma(\pi)$ mas	Ref. ^a	Iso. ^b	CCDM ^c
						Hipparcos	Spectroscopic					
HR 5423	0.15	0.93	6.36	4.50	5545	4.22	3.88	42.43	0.59	0	1	
HR 5447	-0.41	1.02	4.47	3.52	6734	4.21	4.31	64.66	0.72	0	1	14347+2945
HR 5542	0.09	1.04	6.30	3.29	5896	3.82	3.98	24.99	0.80	0	1	
HR 5691	-0.02	1.04	5.15	3.13	6077	3.81	3.94	39.51	0.47	0	1	
HR 5698	-0.01	1.05	4.99	2.32	6245	3.52	3.76	29.27	0.76	0	1	
HR 5723	-0.16	1.05	4.92	2.37	6416	3.58	3.80	30.90	0.99	0	1	
HR 5868	-0.04	0.98	4.42	4.07	5847	4.16	4.06	85.08	0.80	0	1	
HR 5908	-0.06	1.05	4.13	0.64	4865	2.34	2.60	20.02	0.88	1	1	
HR 5908	0.00	1.05	4.13	0.64	4780	2.31	2.49	20.02	0.88	2	1	
HR 5914	-0.46	1.01	4.60	3.60	5831	3.99	3.96	63.08	0.54	0	1	
HR 5933	-0.18	1.01	3.85	3.62	6268	4.12	4.04	89.92	0.72	0	1	15564+1540
HR 5968	-0.22	0.97	5.39	4.18	5745	4.17	4.11	57.38	0.71	0	1	16011+3318
HR 5996	0.27	0.98	6.32	4.02	5756	4.12	4.10	34.60	1.00	0	1	
HR 6189	-0.53	0.93	6.33	3.14	6170	3.78	4.12	23.02	0.89	0	0	
HR 6202	-0.32	1.05	5.55	2.41	6465	3.61	4.02	23.50	1.05	0	1	16419-1955
HR 6243	-0.03	1.05	4.64	1.80	6361	3.33	3.55	27.04	1.08	0	1	
HR 6315	-0.18	0.98	4.88	3.99	6215	4.24	4.01	66.28	0.48	0	1	
HR 6409	0.02	1.05	5.53	2.01	6233	3.38	3.54	19.80	0.72	0	1	
HR 6458	-0.38	0.92	5.38	4.59	5633	4.28	4.12	69.48	0.56	0	1	17206+3229
HR 6541	-0.21	1.04	5.65	2.83	6196	3.71	3.69	27.26	0.73	0	1	
HR 6569	-0.31	1.04	4.76	3.06	6601	3.92	3.99	45.72	0.79	0	1	
HR 6598	-0.33	1.04	6.33	3.19	5757	3.74	3.68	23.53	0.54	0	1	
HR 6649	-0.35	1.01	6.19	3.62	6060	4.06	4.19	30.55	0.90	0	1	
HR 6701	-0.20	1.05	5.02	2.49	6129	3.55	3.75	31.13	0.47	0	1	
HR 6775	-0.54	0.90	5.05	4.08	6001	4.17	4.21	63.88	0.55	0	0	18071+3034
HR 6850	-0.32	1.04	4.99	3.14	6525	3.93	4.05	42.56	0.45	0	1	
HR 6869	-0.10	1.05	3.23	1.84	4930	2.90	3.12	52.81	0.75	1	1	18214-0253
HR 6869	0.00	1.05	3.23	1.84	4950	2.91	2.94	52.81	0.75	2	1	18214-0253
HR 6907	0.07	1.04	5.90	3.10	6245	3.84	4.08	27.53	0.91	0	1	
HR 6913	0.09	1.05	2.82	0.95	4775	2.45	2.73	42.20	0.90	1	1	
HR 7061	-0.09	1.04	4.19	2.79	6301	3.72	3.93	52.37	0.68	0	1	18457+2033
HR 7126	0.15	1.04	5.56	3.03	6517	3.89	4.22	31.24	0.75	0	1	
HR 7232	0.05	0.88	6.15	4.98	5578	4.39	4.23	58.24	0.91	0	1	
HR 7322	-0.29	1.04	6.02	2.88	6254	3.75	3.90	23.57	0.57	0	1	
HR 7534	-0.16	1.02	5.00	3.40	6289	4.04	4.10	47.94	0.54	0	1	19465+3343
HR 7560	0.03	1.01	5.12	3.68	6047	4.08	4.22	51.57	0.77	0	1	19510+1025
HR 7602	-0.13	1.04	3.71	3.03	5225	3.50	3.65	72.95	0.83	1	1	19553+0625
HR 7766	-0.36	1.01	6.26	3.71	5948	4.06	4.07	30.84	0.88	0	1	
HR 7875	-0.40	1.04	5.11	3.19	6031	3.82	4.05	41.33	0.73	0	1	
HR 7955	0.07	1.05	4.52	2.35	6064	3.48	3.81	36.87	0.46	0	1	20454+5735
HR 8027	-0.37	1.02	5.76	3.48	6246	4.06	4.27	35.07	0.83	0	1	
HR 8041	0.13	0.97	6.21	4.10	5734	4.14	3.83	37.80	1.01	0	1	
HR 8077	-0.08	1.04	5.94	3.10	6095	3.80	3.90	27.06	1.07	0	1	21054+0558
HR 8181	-0.62	0.87	4.21	4.39	6244	4.35	4.62	108.50	0.59	0	0	
HR 8354	-0.59	0.92	5.52	3.31	6378	3.91	4.11	36.15	0.69	0	0	
HR 8472	0.03	1.05	5.24	2.40	6160	3.52	3.76	27.03	0.49	0	1	22119+5650
HR 8665	-0.30	1.04	4.20	3.15	6184	3.84	3.92	61.54	0.77	0	1	22467+1211

Table 1—Continued

Star	[Fe/H]	Mass M _⊙	V	M _v	T _{eff} K	log g Hipparcos	log g Spectroscopic	π mas	σ(π) mas	Ref. ^a	Iso. ^b	CCDM ^c
HR 8697	-0.23	1.04	5.16	3.02	6250	3.81	4.14	37.25	0.76	0	1	
HR 8729	0.08	0.93	5.45	4.52	5669	4.27	4.06	65.10	0.76	0	1	
HR 8805	-0.17	1.04	5.68	3.02	6502	3.87	4.08	29.33	0.62	0	1	
HR 8853	-0.02	0.98	5.58	4.04	6067	4.22	4.08	49.31	0.58	0	1	23167+5313
HR 8885	-0.01	1.04	5.77	2.63	6443	3.70	3.78	23.59	0.77	0	1	23208+3810
HR 8969	-0.17	1.02	4.13	3.43	6198	4.03	4.28	72.51	0.88	0	1	23399+0538
HD 400	-0.26	1.01	6.21	3.61	6156	4.09	3.98	30.26	0.69	3	1	
HD 2615	-0.54	0.93	7.62	3.22	6324	3.86	4.11	13.20	0.93	0	0	
HD 6434	-0.53	0.86	7.72	4.69	5796	4.34	4.42	24.80	0.89	0	0	
HD 14938	-0.33	1.02	7.20	3.55	6180	4.07	4.04	18.58	1.11	0	1	
HD 17548	-0.54	0.87	8.16	4.54	6015	4.35	4.46	18.90	1.38	0	0	
HD 18768	-0.51	0.93	6.72	3.40	5769	3.77	4.00	21.65	0.82	0	0	
HD 19445	-1.97	0.75	8.04	5.10	6040	4.51	4.12	25.85	1.14	3	0	
HD 19445	-2.30	0.75	8.04	5.10	5880	4.46	4.10	25.85	1.14	4	1	
HD 19445	-1.88	0.76	8.04	5.10	6080	4.52	4.72	25.85	1.14	0	0	
HD 19445	-1.89	0.76	8.04	5.10	6052	4.51	4.78	25.85	1.14	0	0	
HD 22879	-0.76	0.83	6.68	4.75	5926	4.38	4.57	41.07	0.86	0	0	
HD 25329	-1.69	0.58	8.51	7.18	4849	4.77	4.65	54.14	1.08	0	0	
HD 25704	-0.79	0.85	8.11	4.51	5903	4.29	4.49	19.02	0.87	0	0	04017-5712
HD 30649	-0.46	0.93	6.94	4.56	5789	4.32	4.32	33.44	1.12	0	1	04518+4550
HD 30743	-0.42	1.02	6.27	3.53	6295	4.09	3.73	28.28	0.80	3	1	
HD 30743	-0.48	0.93	6.27	3.53	6288	3.98	3.80	28.28	0.80	3	0	
HD 34328	-1.90	0.74	9.43	5.24	5830	4.50	4.25	14.55	1.01	4	0	
HD 34328	-1.44	0.76	9.43	5.24	5986	4.55	4.89	14.55	1.01	0	0	
HD 38007	-0.30	1.02	6.85	3.55	5671	3.92	4.04	21.89	0.88	0	1	
HD 43947	-0.27	0.94	6.61	4.41	5966	4.32	4.51	36.32	0.90	0	1	
HD 51929	-0.59	0.87	7.39	4.51	5876	4.29	4.47	26.58	0.55	0	0	
HD 59984	-0.64	0.92	5.90	3.52	5911	3.87	4.06	33.40	0.93	0	0	07321-0853
HD 61421	0.01	1.04	0.40	2.68	6470	3.73	3.58	285.93	0.88	3	1	07393+0514
HD 62301	-0.60	0.90	6.74	4.07	5948	4.15	4.19	29.22	0.96	0	0	
HD 62644	0.03	1.04	5.04	3.13	5294	3.56	3.41	41.43	0.81	0	1	
HD 64090	-1.60	0.68	8.27	6.01	5515	4.66	4.99	35.29	1.04	0	0	07536+3037
HD 64606	-0.93	0.72	7.43	6.01	5206	4.57	4.57	52.01	1.85	0	0	07546-0125
HD 66573	-0.53	0.84	7.26	4.91	5739	4.39	4.42	33.88	1.17	0	0	
HD 68284	-0.55	0.93	7.75	3.40	5912	3.81	4.02	13.47	1.17	0	0	
HD 69611	-0.55	0.89	7.74	4.29	5808	4.20	4.47	20.46	1.16	0	0	
HD 74011	-0.57	0.90	7.42	4.08	5776	4.11	4.15	21.51	0.95	0	0	
HD 78558	-0.40	0.94	7.29	4.47	5736	4.27	4.41	27.27	0.91	0	1	
HD 78747	-0.62	0.85	7.72	4.72	5830	4.35	4.45	25.16	0.68	0	0	
HD 84937	-2.04	0.83	8.33	3.80	6344	4.13	4.06	12.44	1.06	0	0	
HD 84937	-2.10	0.83	8.33	3.80	6357	4.13	4.14	12.44	1.06	0	0	
HD 84937	-2.40	0.82	8.33	3.80	6200	4.09	3.60	12.44	1.06	4	1	
HD 91324	-0.23	1.04	4.89	3.19	6150	3.85	3.89	45.72	0.51	0	1	10314-5343
HD 91347	-0.45	0.91	7.50	4.72	5901	4.40	4.28	27.79	0.82	0	1	
HD 94028	-1.38	0.80	8.21	4.63	6060	4.36	4.54	19.23	1.13	0	0	
HD 98553	-0.41	0.89	7.54	4.89	5905	4.46	4.58	29.47	0.89	0	1	
HD 102365	-0.08	0.87	4.89	5.06	5637	4.44	4.45	108.23	0.70	0	1	

Table 1—Continued

Star	[Fe/H]	Mass M _⊙	V	M _v	T _{eff} K	log g Hipparcos	log g Spectroscopic	π mas	σ(π) mas	Ref. ^a	Iso. ^b	CCDM ^c
HD 108177	-1.55	0.78	9.66	4.86	6178	4.47	4.50	10.95	1.29	0	0	
HD 114762	-0.67	0.88	7.30	4.26	5941	4.22	4.17	24.65	1.44	0	0	
HD 114946	0.12	1.05	5.31	2.38	5198	3.22	3.72	25.89	0.73	0	1	
HD 116064	-1.86	0.78	8.80	4.76	5983	4.37	4.58	15.54	1.44	0	0	13217-3919
HD 116064	-2.30	0.78	8.80	4.76	5850	4.33	3.70	15.54	1.44	4	1	13217-3919
HD 121384	-0.34	1.04	6.00	3.09	5199	3.52	3.70	26.24	0.67	0	1	13565-5442
HD 126512	-0.56	0.91	7.27	3.91	5784	4.05	3.97	21.32	0.83	0	0	
HD 126681	-1.09	0.73	9.28	5.69	5625	4.60	4.95	19.16	1.44	0	0	
HD 130551	-0.55	0.92	7.16	3.76	6307	4.14	4.40	20.94	0.88	0	0	
HD 134169	-0.68	0.90	7.67	3.80	5872	4.02	4.18	16.80	1.11	0	0	
HD 134169	-0.76	0.89	7.67	3.80	5887	4.02	4.30	16.80	1.11	0	0	
HD 136352	-0.21	0.90	5.65	4.83	5695	4.38	4.54	68.70	0.79	0	1	
HD 140283	-2.38	0.84	7.20	3.41	5755	3.81	3.66	17.44	0.97	0	1	
HD 140283	-2.41	0.84	7.20	3.41	5779	3.81	3.79	17.44	0.97	0	1	
HD 140283	-2.42	0.84	7.20	3.41	5763	3.81	3.60	17.44	0.97	0	1	
HD 140283	-2.34	0.84	7.20	3.41	5843	3.83	3.20	17.44	0.97	3	1	
HD 140283	-2.54	0.84	7.20	3.41	5750	3.80	3.40	17.44	0.97	5	1	
HD 140283	-2.70	0.84	7.20	3.41	5640	3.77	3.10	17.44	0.97	4	1	
HD 144172	-0.44	1.04	6.81	3.23	6324	3.92	4.10	19.25	0.90	0	1	
HD 148211	-0.61	0.89	7.69	4.08	5921	4.15	4.35	18.98	0.98	0	0	
HD 148816	-0.68	0.88	7.27	4.20	5928	4.19	4.39	24.34	0.90	0	0	
HD 155358	-0.61	0.89	7.28	4.09	5914	4.15	4.09	23.04	0.69	0	0	
HD 157089	-0.51	0.91	6.95	4.01	5833	4.10	4.35	25.88	0.95	0	0	
HD 159307	-0.68	0.92	7.40	3.04	6278	3.77	4.03	13.40	0.99	0	0	
HD 165401	-0.44	0.90	6.80	4.86	5734	4.40	4.33	41.00	0.88	0	1	
HD 166913	-1.44	0.82	8.22	4.25	6175	4.25	4.61	16.09	1.04	0	0	
HD 166913	-1.80	0.81	8.22	4.25	6030	4.21	3.90	16.09	1.04	4	0	
HD 174912	-0.46	0.91	7.15	4.76	5894	4.42	4.19	33.31	0.61	0	1	
HD 181743	-1.66	0.77	9.68	4.95	6080	4.47	4.86	11.31	1.76	0	0	
HD 181743	-2.00	0.77	9.68	4.95	5910	4.42	4.25	11.31	1.76	4	0	
HD 184499	-0.53	0.90	6.62	4.10	5750	4.11	3.98	31.29	0.62	0	0	
HD 187691	0.08	1.01	5.12	3.68	6074	4.09	4.06	51.57	0.77	3	1	19510+1025
HD 188510	-1.37	0.71	8.83	5.85	5628	4.64	5.16	25.32	1.17	0	0	
HD 188815	-0.54	0.92	7.47	3.72	6201	4.06	4.38	17.82	1.05	0	0	
HD 193901	-1.00	0.76	8.65	5.45	5796	4.58	4.79	22.88	1.24	0	0	
HD 194598	-1.01	0.83	8.33	4.60	6047	4.36	4.65	17.94	1.24	0	0	
HD 194598	-1.03	0.83	8.33	4.60	6047	4.35	4.34	17.94	1.24	0	0	
HD 194598	-1.11	0.82	8.33	4.60	6050	4.35	4.19	17.94	1.24	3	0	
HD 194598	-1.40	0.80	8.33	4.60	5920	4.31	4.10	17.94	1.24	4	0	
HD 198044	-0.28	1.00	7.31	3.82	6101	4.15	4.06	20.09	0.94	0	1	
HD 199289	-0.99	0.82	8.28	4.67	5936	4.35	4.71	18.94	1.03	0	0	
HD 201099	-0.47	0.91	7.59	4.10	5898	4.16	4.24	20.09	1.02	0	0	21077-0534
HD 201891	-0.94	0.83	7.37	4.63	5974	4.35	4.97	28.26	1.01	0	0	
HD 201891	-1.05	0.82	7.37	4.63	5948	4.34	4.14	28.26	1.01	3	0	
HD 205294	-0.36	1.04	6.86	3.23	6234	3.89	4.09	18.78	0.86	0	1	
HD 208906	-0.65	0.85	6.95	4.62	6072	4.38	4.47	34.12	0.70	0	0	21587+2949
HD 210752	-0.59	0.86	7.44	4.56	5958	4.34	4.59	26.57	0.85	0	0	

Table 1—Continued

Star	[Fe/H]	Mass M _⊙	V	M _v	T _{eff} K	log g Hipparcos	log g Spectroscopic	π mas	σ(π) mas	Ref. ^a	Iso. ^b	CCDM ^c
HD 215257	-0.62	0.88	7.41	4.28	6002	4.25	4.45	23.66	0.97	0	0	
HD 218504	-0.58	0.89	8.11	4.16	5971	4.19	4.37	16.20	1.01	0	0	
HD 221830	-0.45	0.95	6.86	4.31	5719	4.21	4.13	30.93	0.73	0	1	
BD+21 0607	-1.57	0.79	9.23	4.77	6139	4.43	4.38	12.84	1.33	0	0	
BD+26 2606	-2.29	0.77	9.73	4.79	6146	4.43	4.23	10.28	1.42	0	1	
BD+29 2091	-1.89	0.73	10.26	5.38	5921	4.57	4.72	10.55	1.75	0	0	
BD+51 1696	-1.26	0.73	9.91	5.58	5708	4.58	4.87	13.61	1.54	0	0	
BD+54 1216	-1.49	0.79	9.73	4.81	6116	4.43	4.62	10.36	1.47	0	0	

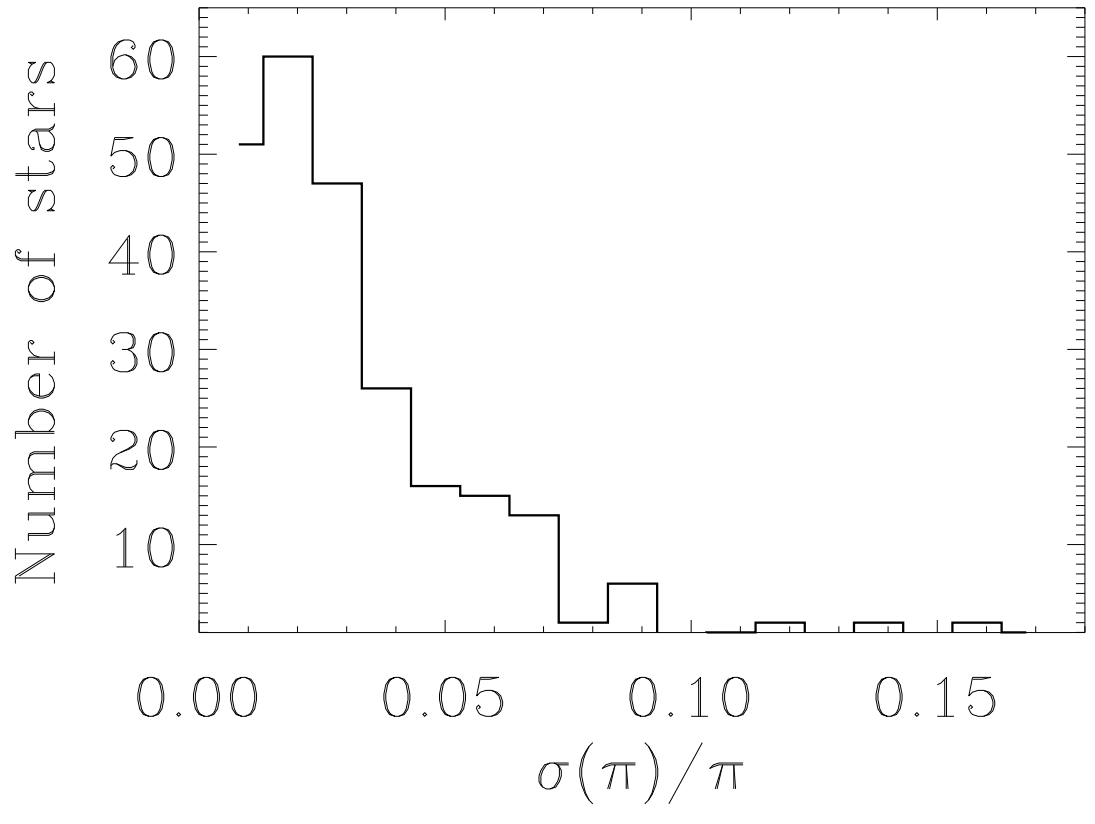
^aReference code; 0: Gratton et al. 1997, 1: Edvardsson 1998, 2: Bonnell & Bell 1993, 3: Fuhrmann et al. 1997, 4: Magain 1989, 5: Ryan, Norris & Beers 1996

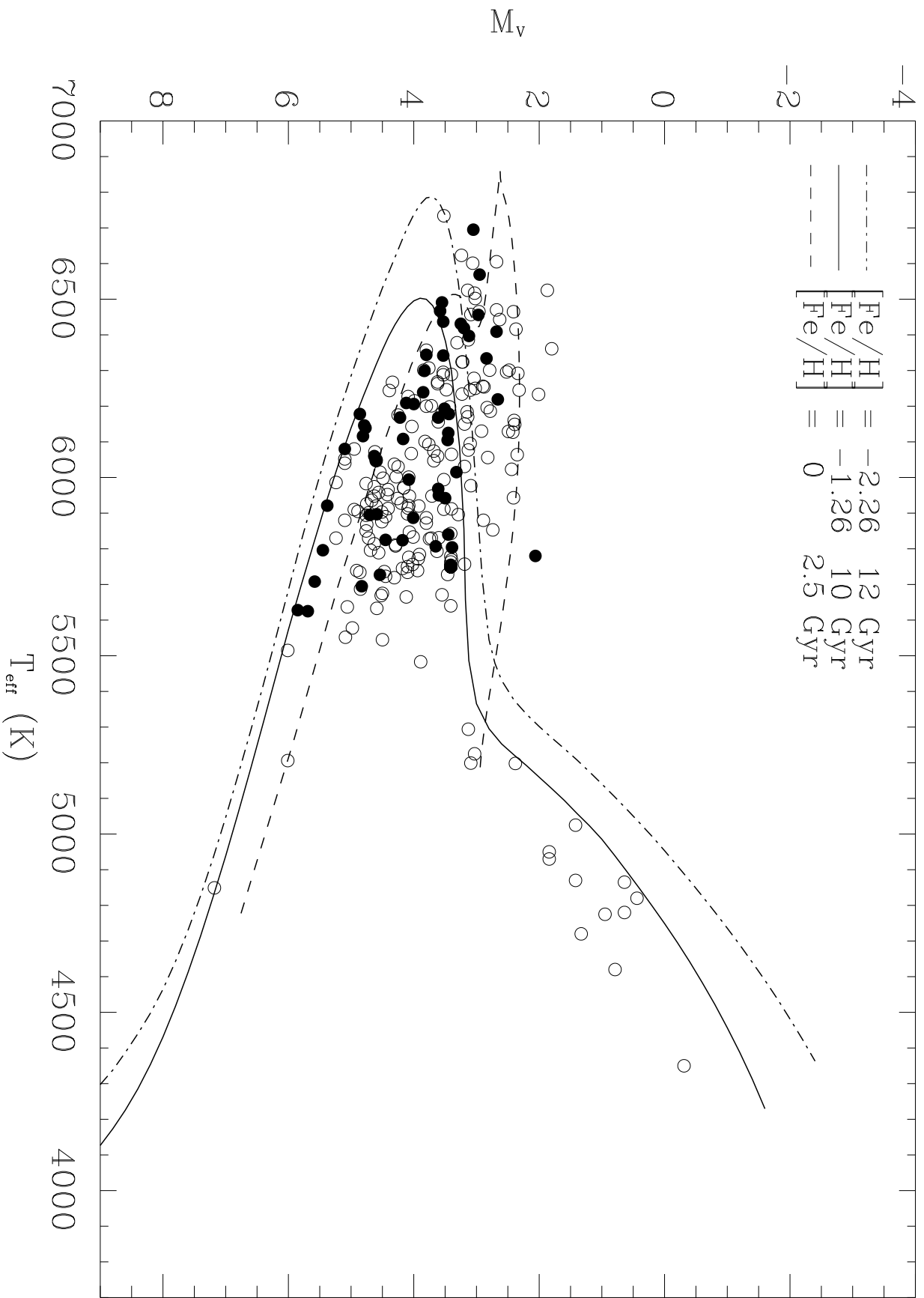
^bIsochrone code; 0: within the metallicity range of Bergbusch & Vandenberg 1992; 1: [Fe/H] too low ([Fe/H]=−2.26 is assumed in the grid of Bergbusch & Vandenberg 1992) or [Fe/H] too high ([Fe/H]=−0.47 is used)

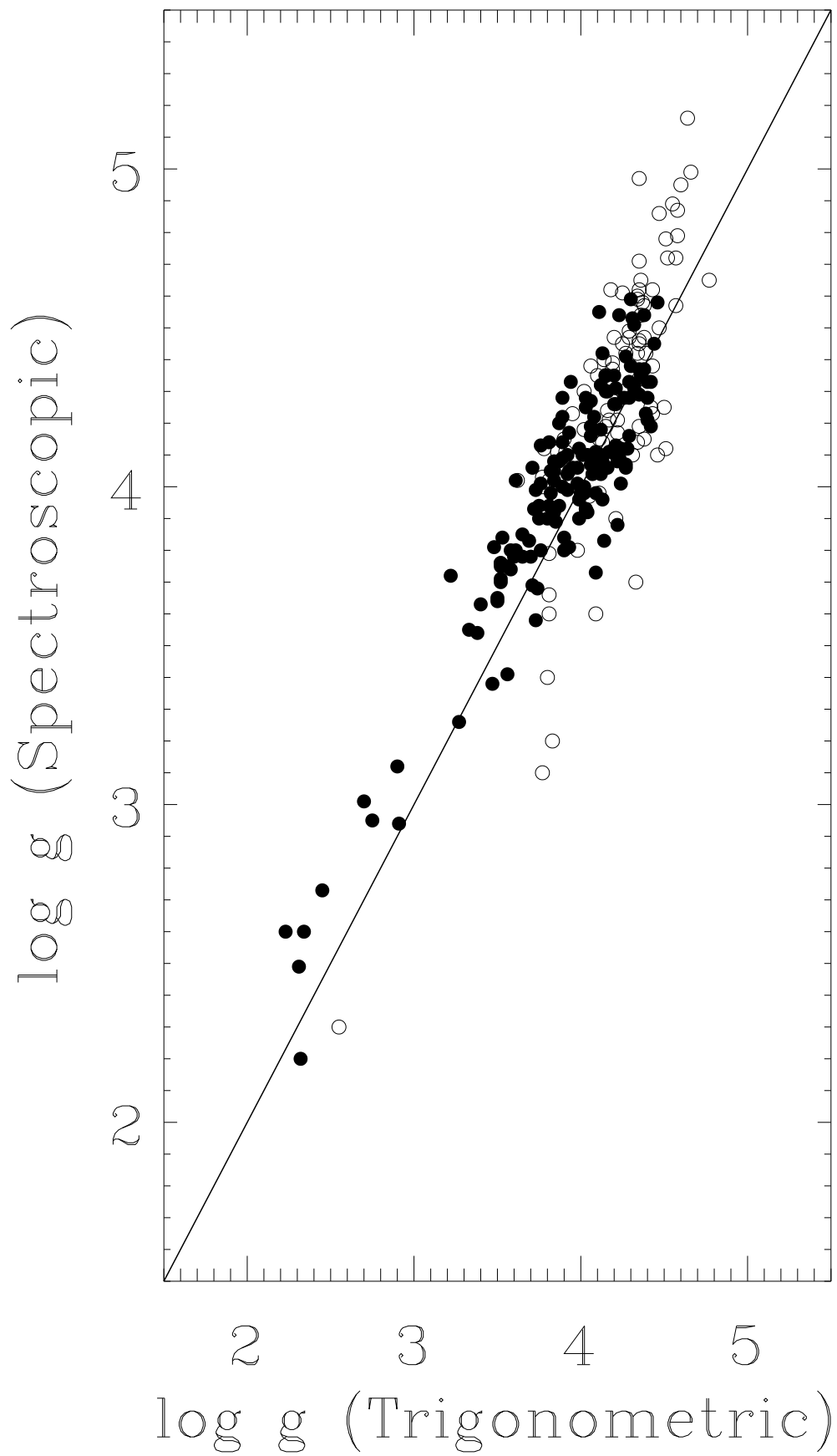
^cComponents of Double and Multiple stars: Dommanget & Nys 1994

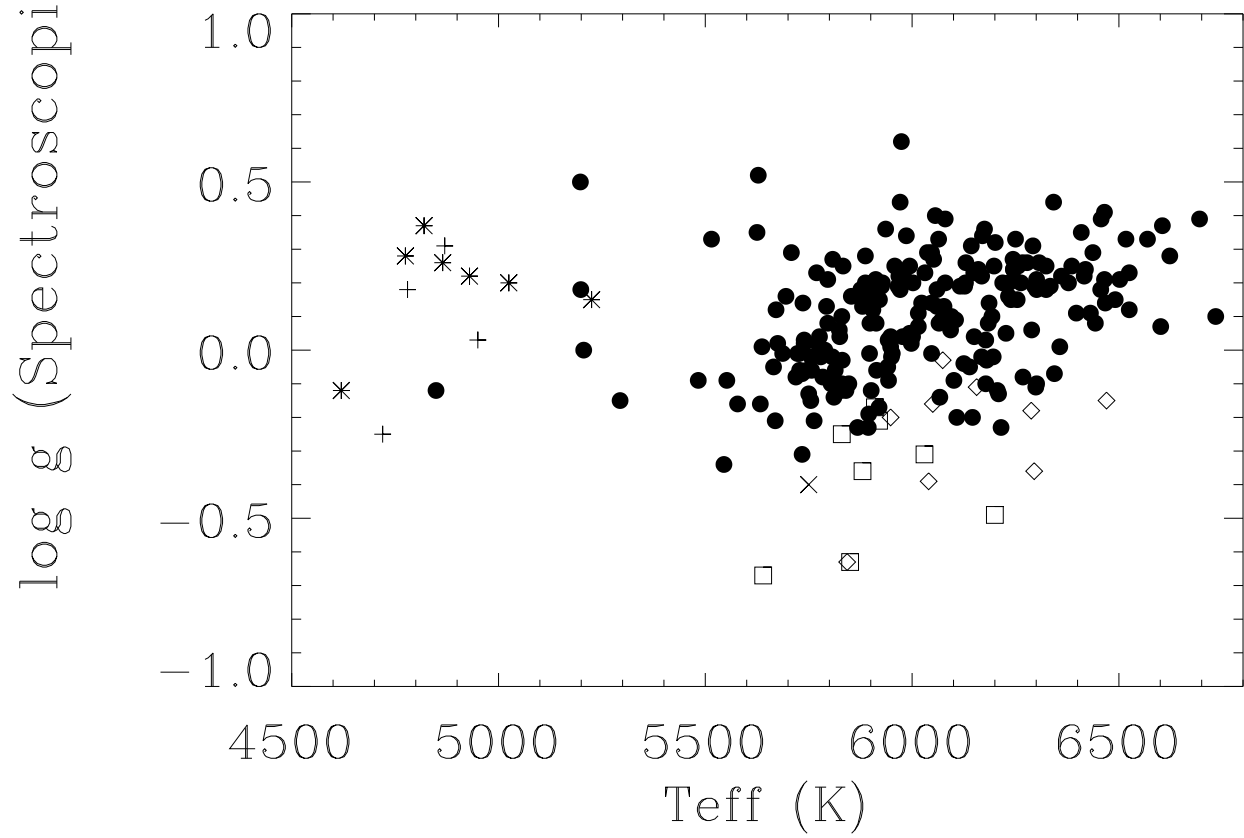
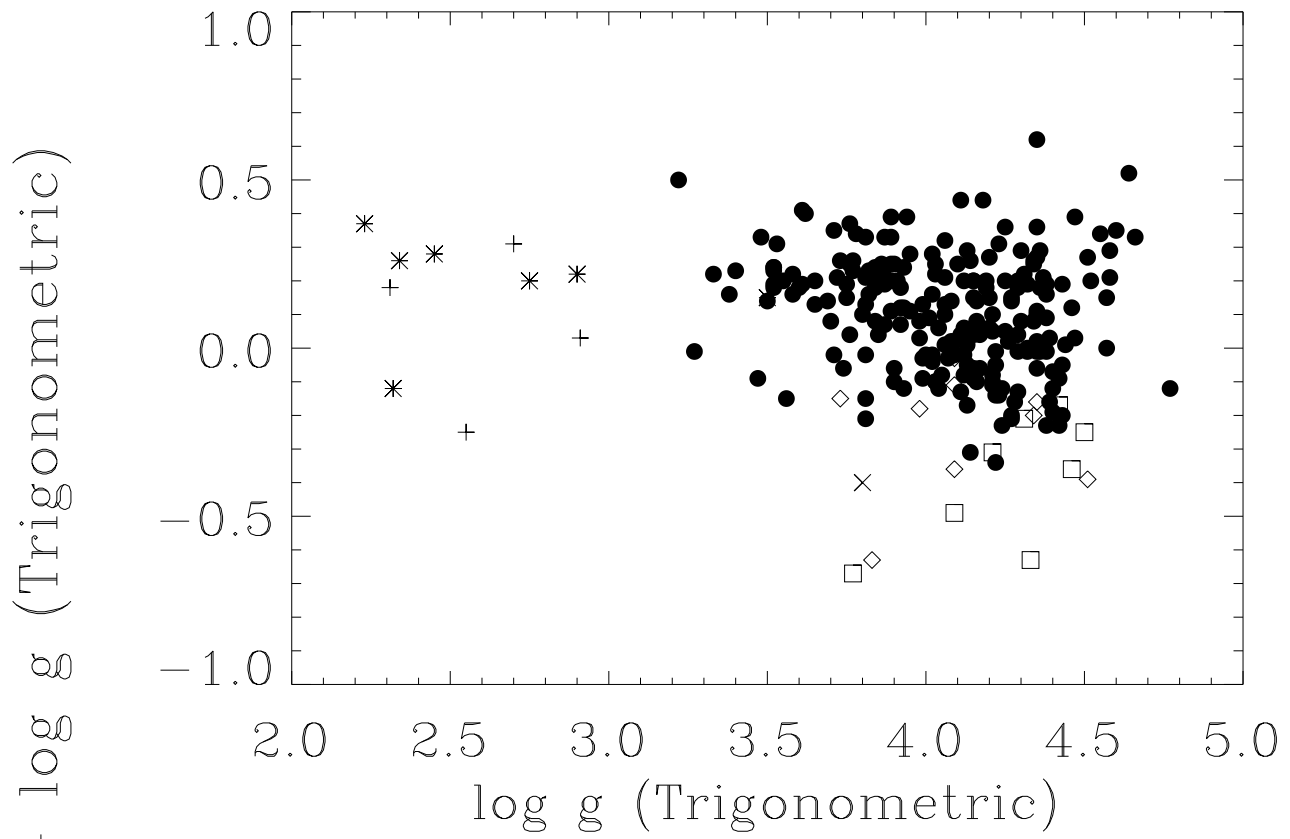
Table 2. Mean difference and standard deviation between spectroscopic and trigonometric gravities

Reference	<[Fe/H]>	< Δ log g >	Number of stars
Edvardsson (1988)	+0.01 ± 0.11	+0.19 ± 0.15	7
Bonnell & Bell (1993)	−0.20 ± 0.27	+0.13 ± 0.25	4
Gratton et al. (1996)	−0.42 ± 0.55	+0.11 ± 0.17	214
Fuhrmann et al. (1997)	−0.84 ± 0.86	−0.25 ± 0.18	9
Magain (1989)	−2.10 ± 0.41	−0.39 ± 0.19	8
Ryan et al. (1996)	−2.54	−0.40	1

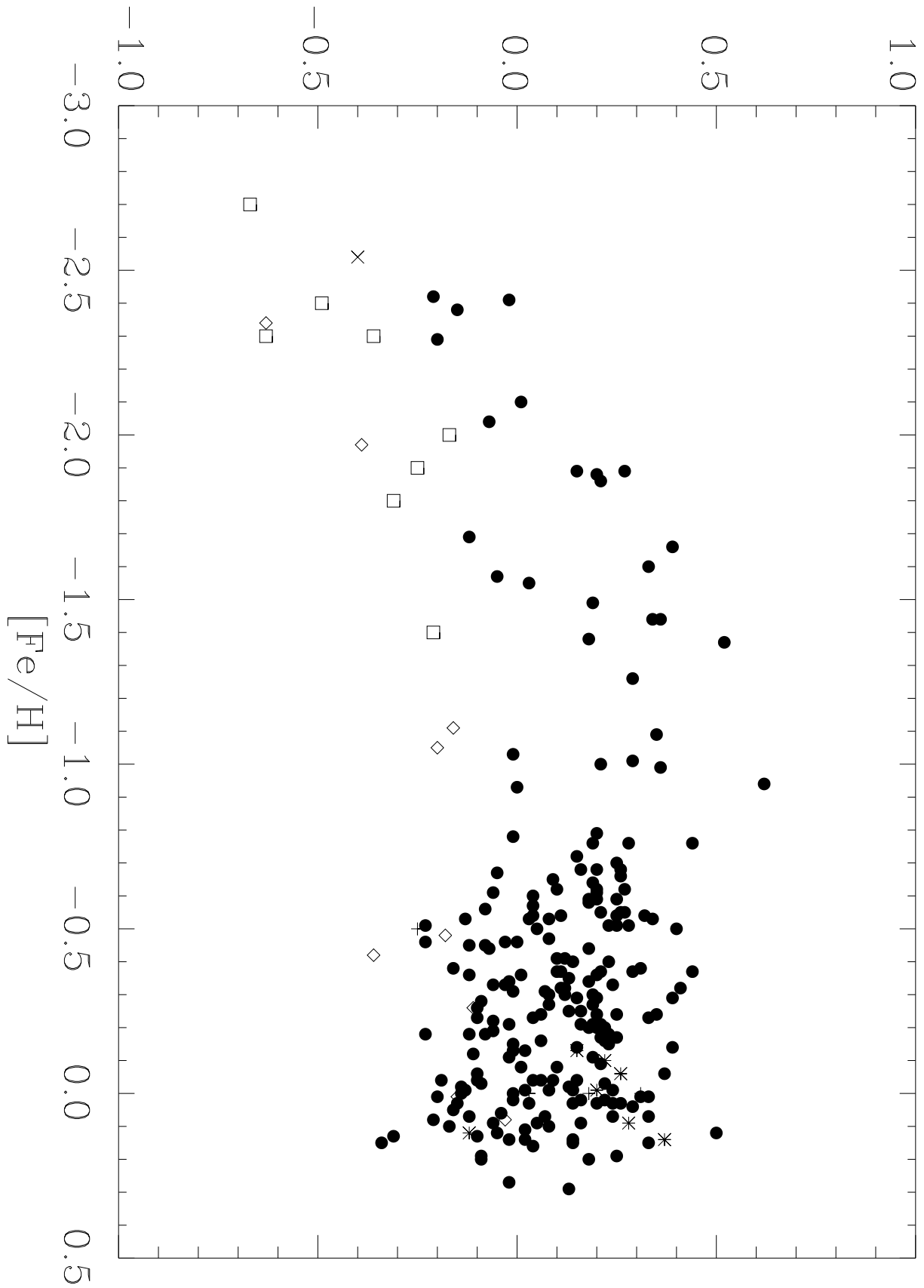


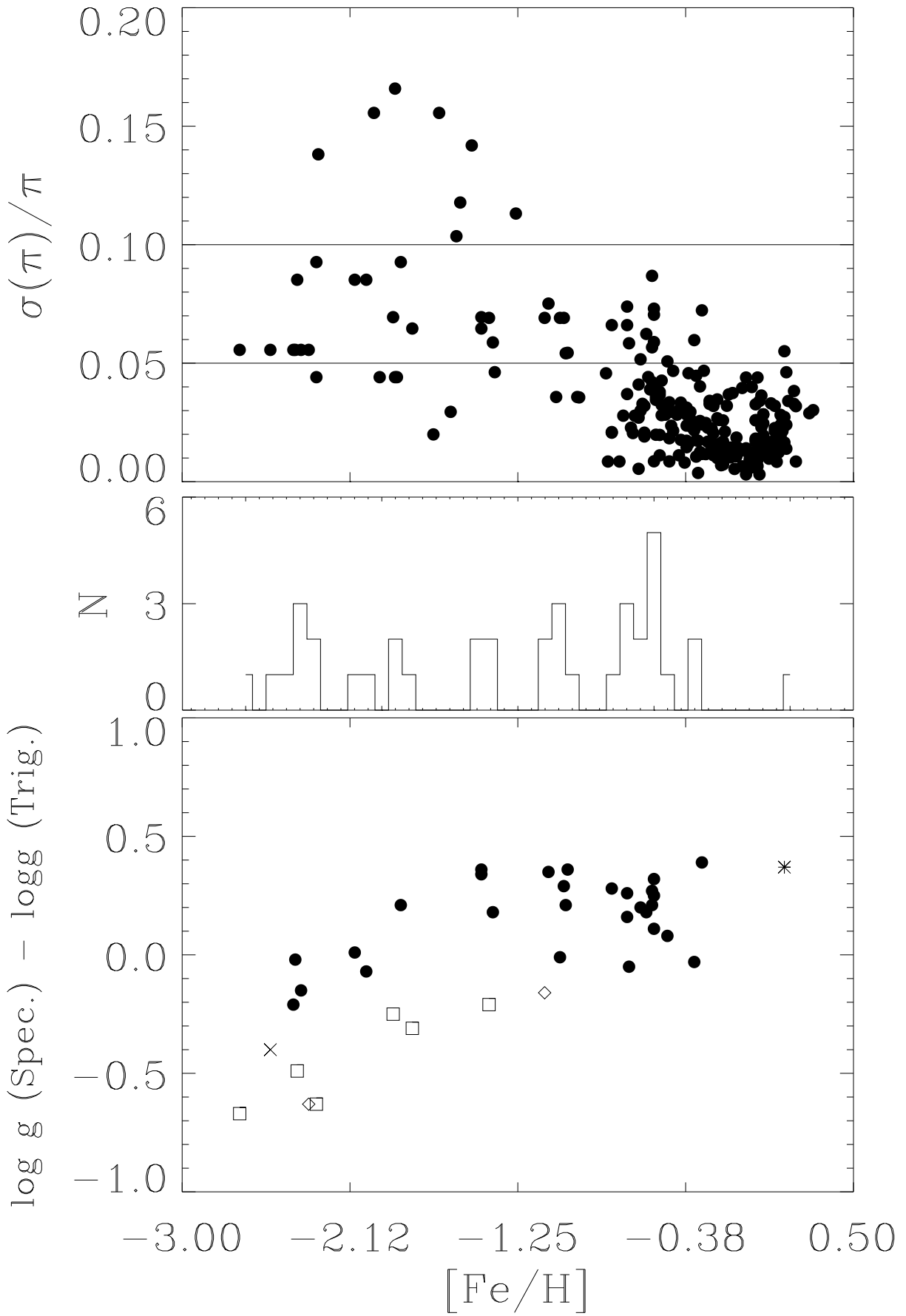


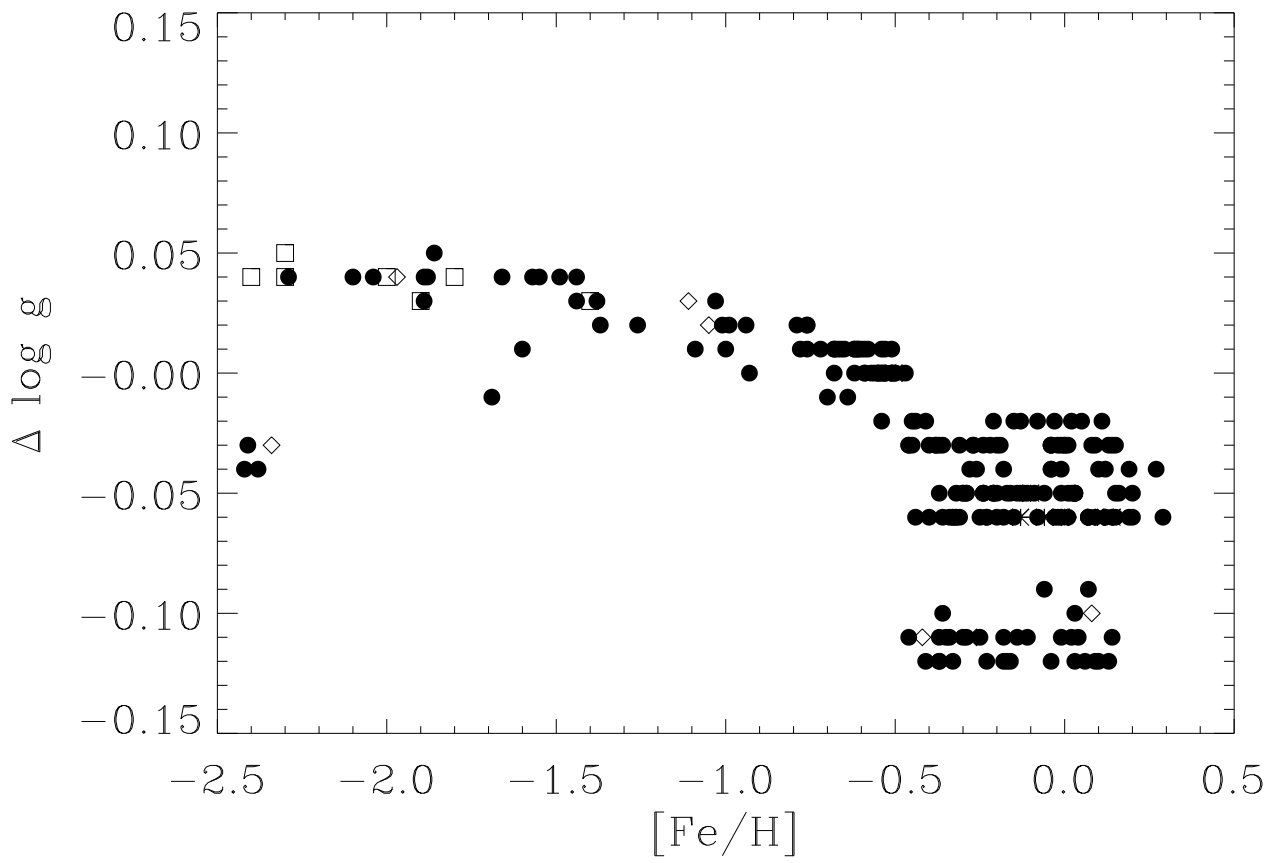
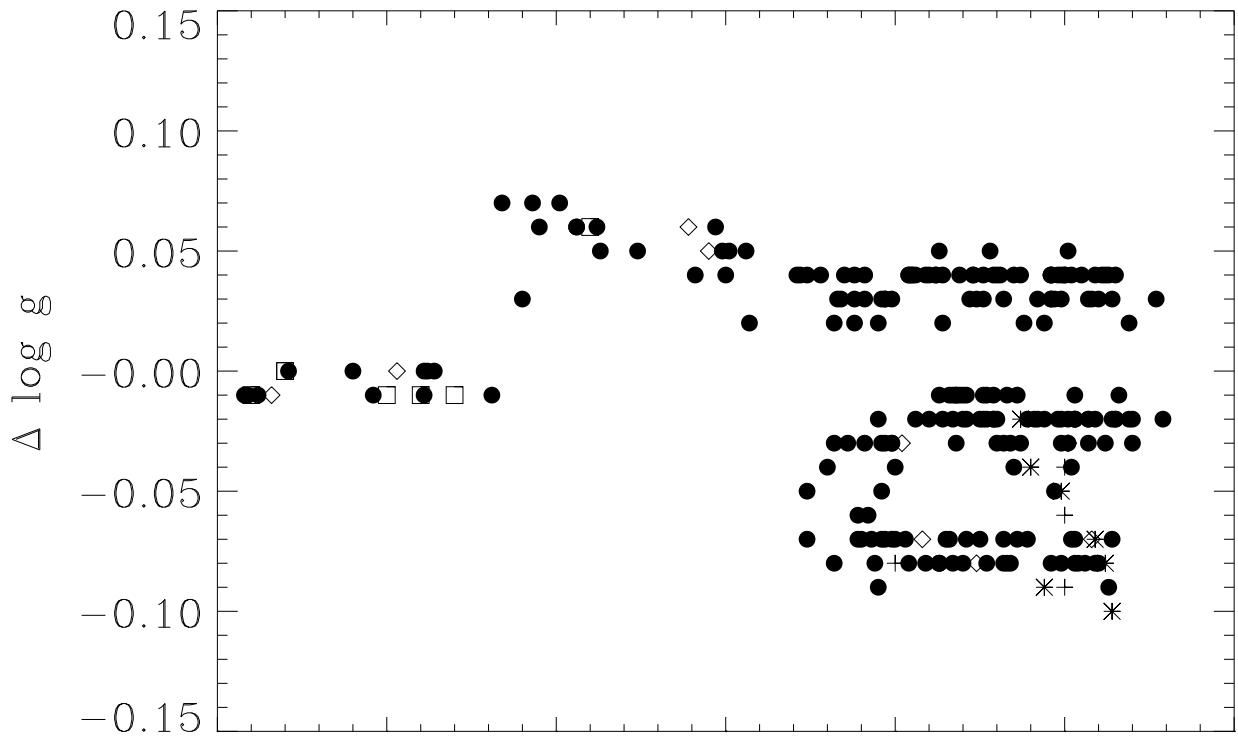




$\log g$ (Spectroscopic) - $\log g$ (Trigonometric)







$\log g$ (Spectroscopic) - $\log g$ (Trigonometric)

